environmental microbiology

Environmental Microbiology (2019) **21**(12), 4773–4791 doi:10.1111/1462-2920.14819

Two genes in a pathogenicity gene cluster encoding secreted proteins are required for appressorial penetration and infection of the maize anthracnose fungus *Colletotrichum graminicola*

Iris Eisermann,[1†] Fabian Weihmann,[1†] Jorrit-Jan Krijger,[1] Christian Kröling,[1,2] Gerd Hause,[3] Matthias Menzel,[4] Silke Pienkny,[5] Andreas Kiesow,[4] Holger B. Deising[1] and Stefan G. R. Wirsel[1*]

[1]*Institut für Agrar- und Ernährungswissenschaften, Naturwissenschaftliche Fakultät III, Martin-Luther-Universität Halle-Wittenberg, Betty-Heimann-Str. 3, D-06120, Halle (Saale), Germany.*

[2]*Sächsisches Landesamt für Umwelt, Landwirtschaft und Geologie, Abteilung Obst-, Gemüse- und Weinbau, August-Böckstiegel-Str. 1, D-01326, Dresden-Pillnitz, Germany.*

[3]*Biozentrum der Martin-Luther-Universität Halle-Wittenberg, Weinbergweg 22, D-06120, Halle (Saale), Germany.*

[4]*Fraunhofer-Institut für Mikrostruktur von Werkstoffen und Systemen, Biologische und makromolekulare Materialien, Walter-Hülse-Str. 1, D-06120, Halle (Saale), Germany.*

[5]*Department of Bioorganic Chemistry, Leibniz Institute of Plant Biochemistry, Weinberg 3, D-06120, Halle (Saale), Germany.*

Summary

To avoid pathogen-associated molecular pattern recognition, the hemibiotrophic maize pathogen *Colletotrichum graminicola* secretes proteins mediating the establishment of biotrophy. Targeted deletion of 26 individual candidate genes and seven gene clusters comprising 32 genes of *C. graminicola* identified a pathogenicity cluster (*CLU5*) of five co-linear genes, all of which, with the exception of *CLU5b*, encode secreted proteins. Targeted deletion of all genes of *CLU5* revealed that *CLU5a* and *CLU5d* are required for full appressorial penetration competence, with virulence deficiencies independent of the host genotype and organ inoculated. Cytorrhysis experiments and microscopy showed that Δ*clu5a* mutants form pressurized appressoria, but they are hampered in forming penetration pores and fail to differentiate a penetration peg. Whereas Δ*clu5d* mutants elicited WT-like papillae, albeit at increased frequencies, papillae induced by Δ*clu5a* mutants were much smaller than those elicited by the WT. Synteny of *CLU5* is not only conserved in *Colletotrichum* spp. but also in additional species of Sordariomycetes including insect pathogens and saprophytes suggesting importance of *CLU5* for fungal biology. Since *CLU5a* and *CLU5d* also occur in non-pathogenic fungi and since they are expressed prior to plant invasion and even in vegetative hyphae, the encoded proteins probably do not act primarily as effectors.

Introduction

Pathogenic fungi face several lines of plant defence that they need to overcome to establish a compatible parasitic interaction (Jones and Dangl, 2006). Activation of pathogen-associated molecular pattern (PAMP)-triggered immune responses is based on the recognition of conserved molecular structures of the attacking pathogen called PAMPs such as chitin, ergosterol and ß-glucans (Lochman and Mikes, 2006; Wan *et al*., 2008; Shetty *et al*., 2009; Oliveira-Garcia and Deising, 2013, 2016). Responses triggered by PAMPs comprise the modification of host cell walls, e.g. the formation of papillae, production of reactive oxygen species, phytoalexins and PR proteins, collectively leading to PAMP-triggered immunity (PTI) (Newman *et al*., 2013). Papillae are callose-containing cell wall appositions localized directly underneath the appressorium, i.e. at sites of attempted fungal penetration (Voigt, 2014). Pathogens adapted to their hosts have evolved means to evade PTI by secretion of effector proteins and/or by avoiding PAMP exposition.

Received 13 June, 2019; revised 1 October, 2019; accepted 2 October, 2019. *For correspondence. E-mail stefan.wirsel@landw.uni-halle.de; Tel. +49 (0)345 5522672; Fax +49 (0)345 5527120. †These authors contributed equally to this work.

Effectors often compromise PTI responses, allowing for disease progression (Oliveira-Garcia and Valent, 2015).

The gene-for-gene hypothesis was established with an obligate biotroph, i.e. the flax rust fungus *Melampsora lini* (Flor, 1971; Ravensdale *et al*., 2011). In the hemibiotrophic maize anthracnose fungus *Colletotrichum graminicola*, races exhibiting differential virulence to maize cultivars have been reported (da Costa *et al*., 2014), but gene-for-gene interactions have not been demonstrated (Nicholson and Warren, 1976). Earlier reports suggested that strategies of evading PTI employed by *C. graminicola* include the reduction of ß-glucan synthesis, interference with chitin-triggered defence responses, and avoidance of secretion of defence-stimulating siderophores at the biotrophic interphase (El Gueddari *et al*., 2002; Oliveira-Garcia and Deising, 2013; Albarouki *et al*., 2014; Oliveira-Garcia and Deising, 2016). In addition to these strategies, *C. graminicola* also relies on secreted proteins to promote infection. Only two of such secreted proteins have yet been functionally characterized in this fungus. Deletion of a gene encoding a secreted protein directed to the hosts' nucleus compromised pathogenicity (Vargas *et al*., 2016), and a secreted metalloprotease that degrades a defence-associated chitinase is required for full virulence (Sanz-Martin *et al*., 2016). This incomplete understanding of defence suppression by this fungus highlights the need to search for further secreted proteins and characterize their roles in disease development. Therefore, we deleted 26 individual candidate genes and seven gene clusters comprising 32 genes of *C. graminicola* and identified two genes located in one cluster, encoding the secreted proteins Clu5a and Clu5d, which are required for appressorial penetration and pathogenicity/virulence.

Table 1. Genes deleted individually.

Gene reference	Annotation	Predicted protein[a]	Size [aa]
YSST1061	GLRG_00416	Hypothetical protein	240
YSST1088	GLRG_00821	Subtilase	401
YSST1135	GLRG_01006	CFEM domain-containing protein (8× Cys)	176
YSST848	GLRG_01439	Hypothetical protein (8× Cys)	192
YSST130	GLRG_01704	Hypothetical protein (8× Cys)	131
YSST1033	GLRG_02090	Hypothetical protein (8× Cys)	188
YSST1124	GLRG_02462	CFEM domain-containing protein (8× Cys)	214
YSST1146	GLRG_03376	Multicopper oxidase (putative laccase 1)	574
YSST1031	GLRG_05029	Hypothetical protein (8× Cys)	115
YSST869	GLRG_05284	Hypothetical protein	274
YSST914	GLRG_05336	Hypothetical protein (8× Cys)	388
YSST1049	GLRG_05667	Hypothetical protein (8× Cys)	285
YSST1094	GLRG_06317	Hypothetical protein (lustrin-like)	388
YSST1091	GLRG_06590	Cerato-platanin	138
YSST908	GLRG_08638	Multicopper oxidase (putative laccase 2)	607
YSST878	GLRG_10074	Fungal hydrophobin (hydrophobin class II)	99
YSST1207	GLRG_10167	Hypothetical protein (8× Cys)	165
YSST1204	GLRG_10982	Peptidase family M28	442
YSST152	GLRG_11367	GDSL-like lipase/ acylhydrolase	263
MGG_01748	GLRG_02846	Eukaryotic aspartyl protease	846
MGG_04128	GLRG_05766	Hypothetical protein	534
MGG_13347	GLRG_06842	Integral membrane protein	435
MGG_07973	GLRG_08263	Hypothetical protein	146
MGG_05948	GLRG_08566	Hypothetical protein	277
MGG_07745	GLRG_09350	Hypothetical protein	777
MGG_04685	GLRG_11030	Hypothetical protein	652

YSST refers to genes identified in Krijger *et al*. (2008). MGG refers to genes identified by Jeon *et al*. (2007) that associate with a specific virulence phenotype in a tagged mutant of *M. oryzae* and that have a putative homologue in *C. graminicola* encoding a secreted protein.
a. Taken from the genome database (http://fungi.ensembl.org/Colletotrichum_graminicola/Info/Index). Additional features are given in brackets.

Results

Functional analyses of candidate genes

We adopted three strategies to identify and functionally analyse candidate genes encoding secreted proteins mediating pathogenesis in *C. graminicola*. First, we focused on genes identified by the yeast signal sequence trap (YSST) (Krijger *et al*., 2008). Of these genes, we deleted 19 by replacing the resident locus by a dominant selection marker via double cross-over. The genes selected encode small cysteine-rich and hypothetical proteins, peptidases, laccases as well as proteins with structural functions such as hydrophobins (Table 1; see Fig. 1 for chromosomal locations). For each gene deleted, at least three independent transformants were analysed for their virulence on leaves of *Zea mays* cv. Mikado. However, no visual differences in symptom severity between the mutants and the wild-type (WT) reference were found.

In the second approach, we deduced the secretome in the annotated genome sequence of *C. graminicola* (O'Connell *et al*., 2012) identifying 1780 proteins with signal peptides (SPs) (14.8% of the annotated proteome; Supporting Information Data File 1). Of the proteins that were found by YSST (Krijger *et al*., 2008) and that were represented in the annotated proteome, 90.6% belonged

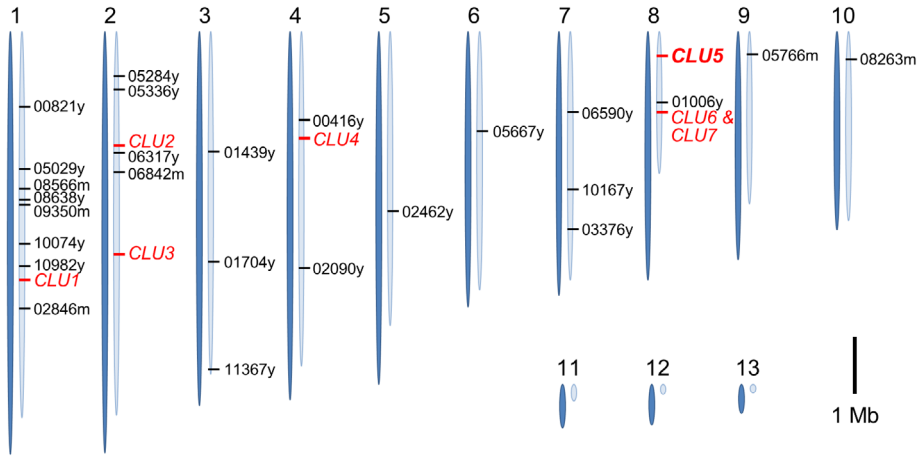

Fig. 1. Chromosomal locations of 25 genes and seven gene clusters analysed. Individual genes are marked with their GLRG-numbers in black, clusters with their number in red. Genes labelled with a 'y' at the end were originally identified by YSST (Krijger *et al*., 2008), whereas the label 'm' refers to genes whose orthologues were identified in *Magnaporthe oryzae* as being needed for full virulence (Jeon *et al*., 2007). Gene GLRG_11030 (Table 1) is not represented, as it locates on an unplaced supercontig. Cluster *CLU5*, deletion of which leads to a loss of pathogenicity, is in boldface. Dark blue ovals represent the chromosome sizes as determined by optical mapping, adding up to 57.4 Mb as reported (O'Connell *et al*., 2012). Light blue ovals represent the chromosome sizes according to the nucleotide assembly.

to the secretome, supporting the bioinformatical procedure. Twenty-nine of the *C. graminicola* genes with an SP were putatively orthologous to mapped virulence genes of *Magnaporthe oryzae* identified by *Agrobacterium tumefaciens* mediated transformation (ATMT) (Jeon *et al*., 2007). We deleted *C. graminicola* genes, whose corresponding ATMT mutants in *M. oryzae* exhibited defects in appressorium formation and virulence (Supporting Information Data File 1). The selected genes encoded five hypothetical proteins with unknown function, an aspartyl protease and an integral membrane protein (Table 1, Fig. 1). Again, none of the deletion mutants exhibited symptom severity that was discernible from the WT.

Since work in the basidiomycete *Ustilago maydis* had indicated that many effector genes are organized into clusters (Kämper *et al*., 2006), we analysed the genome of *C. graminicola* for gene clusters in the third approach. Excluding genes not mapped yet, we searched for such clusters by asking for a minimum of three co-linear genes, all encoding secreted proteins. The 48 gene clusters meeting this criterion encode 155 proteins corresponding to 9.2% of the secretome (Supporting Information Data File 1). The largest cluster comprised five genes. A more relaxed definition asking for a minimum of four co-linear genes allowing one to encode a non-secreted protein identified 83 clusters encoding 283 proteins (16.9% of the secretome). Applying the relaxed criterion, the largest cluster comprised six genes. We deleted five entire gene clusters that matched the strict or both criteria defined above with a preference given to larger clusters (Table 2, Fig. 1, clusters *CLU1*–*CLU5*, Supporting Information Data File 1). In one case, we transformed a construct designed to delete simultaneously two clusters (*CLU6* and *CLU7*), which were separated by only three genes encoding proteins without a predicted SP. In total, these constructs covered 32 genes. None of the deletion mutants of *CLU1* to *CLU4* suffered from a loss of pathogenicity. For the combined clusters *CLU6* and *CLU7*, no transformant carrying a homologous integration at the targeted genomic region could be recovered. Mutants lacking *CLU6*, *CLU7*, or the region separating them (spacer 6/7) were not affected in virulence (Table 2). In contrast, Δ*clu5* deletion mutants were non-pathogenic (Fig. 2A and B; Fig. S1A).

CLU5a *and* CLU5d *are required for full virulence*

Cluster *CLU5* comprises five genes (GLRG_04686 to GLRG_04690) (Fig. 2A, Table 2), designated as *CLU5a* to *CLU5e*. Except for Clu5b (encoded by GLRG_04687), which is a putative integral membrane protein, all proteins belong to the soluble secretome, as predicted by several computer programs such as SignalP, TargetP, Wolf PSort and PredictProtein. To determine, which gene(s) are required for pathogenicity, all five were deleted individually (Fig. S1C–G). Infection assays using excised leaves of maize cv. Mikado revealed that two of the five genes, *CLU5a* (GLRG_04686) and *CLU5d* (GLRG_04689), are important for disease establishment (Fig. 2C). Quantitative assessment of fungal biomass in infected maize by qPCR supported the differences in symptom severity and showed that Δ*clu5a* mutants were non-pathogenic, whereas Δ*clu5d* mutants had clear virulence defects (Fig. 2D; compared with Fig. 2C). Finally,

Table 2. Gene clusters deleted.

Cluster	Size [kb]	Annotation	Predicted protein[a]	SP	Size [aa][b]
CLU1	14	GLRG_01791	Hypothetical protein	yes	329
		GLRG_01792	Glucose sorbosone dehydrogenase	yes	463
		GLRG_01793	Hypothetical protein	yes	133
		GLRG_01794	Hypothetical protein	yes	128
		GLRG_01795	GDSL-like lipase/acylhydrolase	yes	308
CLU2	5	GLRG_06284	Biotrophy-associated secreted protein 2	yes	99
		GLRG_06285	Peptidase family M28	yes	375
		GLRG_06286	Metalloprotease	yes	280
CLU3	13	GLRG_08160	Hypothetical protein	yes	582
		GLRG_08161	Hypothetical protein	yes	302
		GLRG_08162	Hypothetical protein	yes	117
		GLRG_08163	Hypothetical protein	yes	115
CLU4	23	GLRG_03571	Hypothetical protein	yes	73
		GLRG_03572	Hypothetical protein (Zn-finger protein)	no	585
		GLRG_03573	Hypothetical protein	yes	119
		GLRG_03574	Hypothetical protein (protein disulphide)	yes	378
CLU5	23	GLRG_04686	Hypothetical protein (Clu5a)	yes	56
		GLRG_04687	Hypothetical protein (Clu5b)	no	323
		GLRG_04688	S1/P1 nuclease (Clu5c)	yes	304
		GLRG_04689	Hypothetical protein (Clu5d)	yes	478
		GLRG_04690	Hypothetical protein (Clu5e)	yes	350
CLU6	16	GLRG_01061	GMC oxidoreductase	yes	608
		GLRG_01062	GMC oxidoreductase	yes	786
		GLRG_01063	Hypothetical protein	yes	460
		GLRG_01064	Integral membrane protein DUF6	yes	680
Spacer 6/7	5	GLRG_01065	Hypothetical protein	no	218
		GLRG_01066	ATP-NAD kinase	no	465
		GLRG_01067	Hypothetical protein	no	215
CLU7	9	GLRG_01068	FAD binding domain-containing protein	yes	596
		GLRG_01069	Hypothetical protein	yes	385
		GLRG_01070	FAD binding domain-containing protein	yes	493
		GLRG_01071	Endonuclease/exonuclease/phosphatase	yes	307

SP, signal peptide predicted.
a. Taken from the genome database (http://fungi.ensembl.org/Colletotrichum_graminicola/Info/Index). Additional features are given in brackets.
b. Including predicted signal peptides.

mutants were created that carried a deletion affecting four of the five genes, i.e. *CLU5b* to *CLU5e* (Δ*clu5part*; Fig. S1B). Symptoms caused by these mutants were comparable to those caused by the Δ*clu5d* mutants, suggesting that the other genes covered by the larger deletion do not contribute to virulence (Fig. 2B).

To test whether *CLU5a* and *CLU5d* are needed for penetration of intact host surfaces or for later phases of pathogenesis, maize leaves were mechanically wounded before inoculation. On wounded leaves, Δ*clu5* and Δ*clu5part* mutants, as well as mutants lacking genes *CLU5a* and *CLU5d* resembled the WT with respect to symptom severity (Fig. 2E), suggesting that *CLU5a* and *CLU5d* are required for host penetration but not for subsequent biotrophic and necrotrophic colonization of leaves. Complementation experiments confirmed that the pathogenicity/virulence defects observed in the mutants resulted only from deletion of the resident gene (Fig. S2A–C).

To determine whether the host genotype may influence the outcome of infection, we assessed the virulence of the mutants lacking individual genes on three additional maize cultivars differing in susceptibility to *C. graminicola*. As anticipated (Weihmann *et al*., 2016), the WT caused symptoms, the intensity of which decreased from the cultivars Golden Jubilee, to Mikado, Farmtop and B73 (Fig. 2, Fig. S3). On the highly susceptible cultivar Golden Jubilee, the Δ*clu5a* mutants were similarly impeded in virulence as on cultivar Mikado, whereas no symptoms occurred on cultivars Farmtop and B73. The Δ*clu5d* mutants showed stronger symptoms on Golden Jubilee than on Mikado, which, however, remained milder than those caused by the WT. Similarly, on cultivars Farmtop and B73 symptoms caused by Δ*clu5d* mutants were weaker than those caused by the WT. The mutants of the other genes did not differ notably from the WT on any host.

Interestingly, *C. graminicola* not only infects the leaves of maize but also its stalks (Bergstrom and Nicholson, 1999). Using a quantitative infection assay, we analysed virulence of the individual *CLU5* mutants in stalk assays. Inoculation of wounded stalks of maize cultivar Mikado with WT conidia caused strong tissue necroses. Only Δ*clu5a* and Δ*clu5d* mutants caused significantly diminished disease symptoms when compared with the WT (Fig. 2F, G). These results

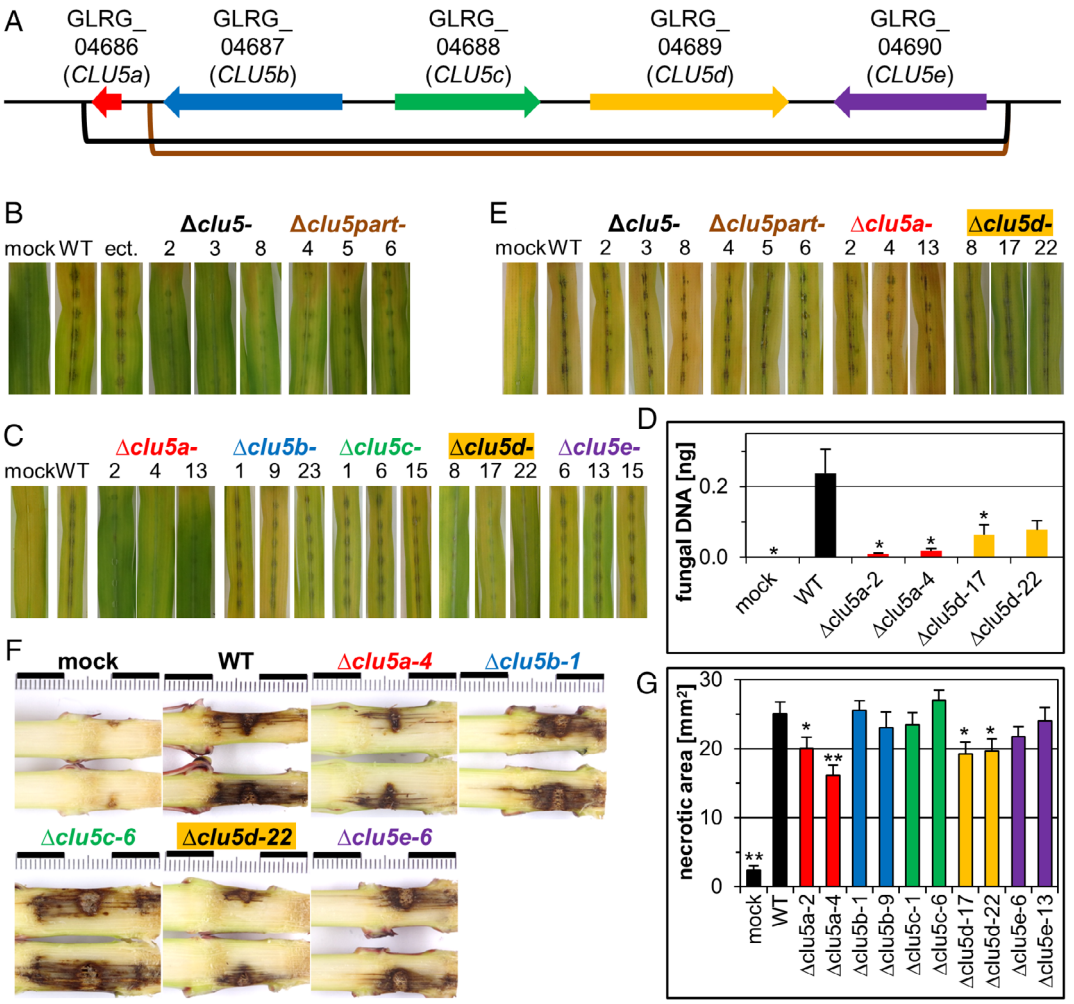

Fig. 2. Identification of genes in cluster *CLU5* contributing to virulence. A. Scheme providing the GLRG numbers and the orientations of the genes, which are drawn to scale. The distances between the genes are not scaled. B., C., E. Representative symptoms occurring on detached leaf segments at 5 dpi. Maize cultivar Mikado was inoculated with 10^4 conidia per spot 14 d after sowing. B. Deletion mutants of the entire cluster and of the partial cluster. C. Deletion mutants of the individual genes. B. and C. used intact leaf surfaces. D. qPCR analysis of DNA isolated from maize cultivar Mikado infected with WT, Δ*clu5a* and Δ*clu5d* strains. Tissues were harvested at 4 dpi. Columns represent the average amount of fungal DNA per reaction ($n = 3$). Error bars show SE, asterisks indicate significant differences between a variant and the WT at $p < 0.05$. E. Deletion mutants of the entire cluster, the partial cluster and of *CLU5a* and *CLU5d* inoculated on wounded leaves. F., G. Virulence on maize stalks. Mutants with individual deletions of *CLU5* genes were inoculated on wounded stalks of maize cultivar Mikado that were harvested at 14 dpi. F. Photographs of representative symptoms. G. Columns represent the means of necrotic areas quantified in longitudinally split stalks ($n = 20$; four biological replications performed at different weeks, each using 5 stalks). Error bars provide SE, one asterisk indicates a significant difference between a variant and the WT at $p < 0.05$, and two asterisks at $p < 0.005$ (unpaired *t*-test).

were similar to those observed in unwounded leaves but not wounded leaves where symptom intensity induced by the mutants was similar to the WT.

Tests assessing *in vitro* fitness penalties possibly resulting from the deletion of individual *CLU5* genes did neither reveal differences to the WT for growth rates on MM/sucrose nor for the formation of conidia (Fig. S4A–C). Substances conferring cell wall (Uvitex 2B, Congo red) or osmotic stress (NaCl, KCl) similarly affected all strains analysed (Fig. S5). Growth at 35°C did neither differentiate the strains (not shown). Microscopy of vegetative hyphae grown *in vitro* on PDA did not exhibit notable differences between the mutants and the WT for septation and branching (not shown). These experiments indicated that diminished virulence of the Δ*clu5a* and Δ*clu5d* mutants does not result from reduced fitness and that *CLU5a* and *CLU5d* are specifically required in pathogenesis.

Bioinformatical analyses of CLU5a *and* CLU5d

The locations of putative orthologues of the *CLU5* genes and those flanking them were determined on contigs/

scaffolds/chromosomes in 14 *Colletotrichum* species with published genome sequences and moreover in *Verticillium dahliae*, *Fusarium graminearum* and *M. oryzae* as more distantly related plant pathogens, as well as in the insect pathogens *Beauveria bassiana* and *Cordyceps militaris*, the saprophytes *Chaetomium thermophilum* and *Neurospora crassa*, and in *Trichoderma harzianum*, which is considered a generalist. All these fungi belong to the class of Sordariomycetes in the Ascomycota. Gene organization was compared with *C. graminicola* only in species for which at least four of eight genes analysed were located on the same scaffold (Fig. 3). Synteny in genomic regions corresponding to cluster *CLU5* is not only well conserved in the *C. graminicola* species complex (*C. sublineola*) but also in members of the closely related *C. destructivum* (*C. higginsianum*) and *C. spaethianum* species complexes (*C. incanum*, *C. tofieldiae*). The other *Colletotrichum* spp. analysed belong to species complexes with a greater phylogenetic distance to *C. graminicola* (Gan *et al*., 2016), and they show some rearrangements at the *CLU5* locus. However, *CLU5b* and *CLU5c* are strictly syntenic and exhibit identical bidirectional promoter organization in all species analysed, except in *M. oryzae* and *B. bassiana* that have genes inserted between them. Strict conservation of position and orientation applies to *CLU5d* in all *Colletotrichum* spp. as well, except *C. simmondsii*. This species and three belonging to other genera have one or two additional genes inserted between *CLU5c* and *CLU5d*. The position of *CLU5a* is conserved in species of the *C. destructivum*, *spaethianum* and *spaethianum* species complexes, whereas it locates in most of the other species somewhere downstream of *CLU5d*. Similarly, the position of *CLU5e*, if present at all, is only well conserved in these species complexes. Taken together, co-linearity at the core of *CLU5* is conserved not only in pathogens of the Glomerellales (*Colletotrichum*, *Verticillium*) but also in additional orders of the Sordariomycetes including insect pathogens and saprophytes (Fig. 3).

Importantly, RNAseq experiments indicated that all *CLU5* genes are transcribed at all stages of pathogenesis (O'Connell *et al*., 2012; Torres *et al*., 2016) (B73 data: J.-J. Krijger *et al*., unpublished) (Fig. S6), with highest transcript levels of *CLU5a* found in *in vitro* differentiated appressoria. *CLU5d* is among the most highly expressed genes in appressoria and biotrophic hyphae *in planta* and is differentially expressed. The latter applies to *CLU5c*, as well (Torres *et al*., 2016). The orthologues of these genes in *C. higginsianum* are also transcribed throughout pathogenesis (O'Connell *et al*., 2012).

CLU5a encodes a small secreted protein with a predicted SP of 18 amino acids (aa) and a mature length of 38 aa. None of the computer programs used revealed known domains or motifs, and no genes encoding similar proteins exist in the genome of *C. graminicola* (Supporting Information Data File 1). However, proteins with similarity to Clu5a exist as single copies in members of the Pezizomycotina class Sordariomycetes, showing not only plant pathogenic but also animal pathogenic (*Metarhizium anisopliae*) and fungi with saprophytic lifestyles (*Neurospora crassa*) (Fig. S7A). The orthologues of *M. oryzae* and *C. orbiculare* have been identified earlier (Saitoh *et al*., 2012).

CLU5d encodes a secreted protein with a predicted SP of 19 amino acids (aa) and a mature length of 436 aa (Schliebner *et al*., 2014). None of the computer programs applied revealed the existence of known domains or motifs in Clu5d (Supporting Information Data File 1). The proteome of *C. graminicola* harbours another protein with some similarity (GLRG_02335, E-value: 2e-71, identity in aligned parts: 51.9%). With the exception of the Saccharomycotina, hypothetical proteins with similarity to Clu5d exist in the Ascomycota, irrespective of the nutritional life style. Related proteins also exist in Basidiomycota (Fig. S7B).

CLU5a *and* CLU5d *mediate appressorial penetration of intact host surfaces*

Light microscopy (LM) of infected leaves of maize cultivar Mikado, stained with Aniline blue, confirmed the assumption (see Fig. 2) that Δ*clu5a* mutants suffered from an appressorial penetration arrest, since no hyphae within epidermal cells were observed (Fig. 4A). In contrast, the WT had formed biotrophic primary hyphae at 2 dpi (Fig. 4A; P) and thinner necrotrophic secondary hyphae at 4 dpi (Fig. 4A; S). Quantification of fungal infection structures showed that conidial germination and appressorium differentiation rates of Δ*clu5a* mutants on maize leaves were similar to those of the WT, but successful penetration events, quantified as the incidence of primary hypha, were extremely rare (Fig. 4B). Investigating Δ*clu5a* mutants on leaves by LM, we did not observe papillae. These defence structures are formed at low frequencies in the compatible interaction of maize with the WT of *C. graminicola* (Weihmann *et al*., 2016). Transmission electron microscopy (TEM) revealed that at 3 dpi, the WT had produced appressoria with a penetration hypha emerging from their bases and penetrating the host cell wall (Fig. 4C; arrow). These invasive hyphae were capable of breaching papillae if such were formed by the host (Fig. 4C; asterisk). In contrast, at the base of appressoria of the Δ*clu5a* mutants, the cell wall appeared thinner suggesting that penetration pore formation has been initiated but not completed and penetration hyphae did not form (Fig. 4D, inserts; arrow). Quantification of penetration pores formed by appressoria, which had

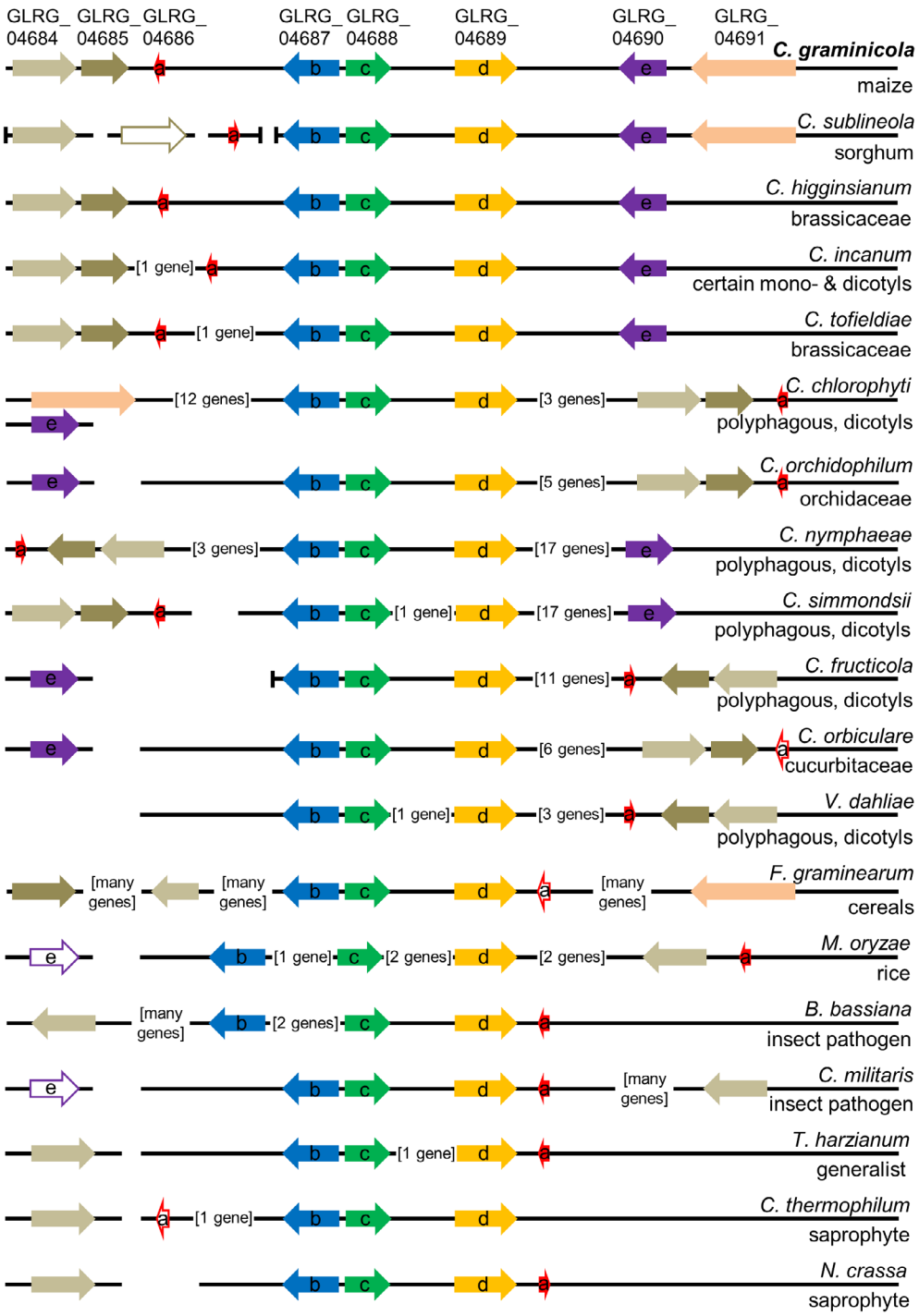

Fig. 3. Synteny of *CLU5*. The orthologues of *CLU5* genes *CLU5a* = GLRG_04686 (a) to *CLU5e* = GLRG_04690 (e) and adjacent genes GLRG_04684 (beige), GLRG_04685 (brown) and GLRG_04691 (rose) and their organization on scaffolds are shown in the monocot pathogens *C. graminicola*, *C. sublineola* and *C. orchidophilum*, and seven *Colletotrichum* spp. infecting dicots. *Colletotrichum incanum* was reported to infect several dicots but also a monocot (Gan *et al*., 2016). Further species were chosen to represent a range of nutrional life styles and orders of the Sordariomycetes. Plant pathogenic species are sorted according to relatedness to *C. graminicola*. Drawing is not to scale. Free scaffold lines (no vertical line) show that the scaffold continues on this side with further genes present. Blocked scaffold lines (vertical line) represent scaffold ends. All species have putative orthologues of GLRG_04691, which reside on separate scaffolds in cases where they are not shown. Genes depicted only with coloured edging were detected in Blast searches with E-values of $\geq 1 \times 10^{-5}$.

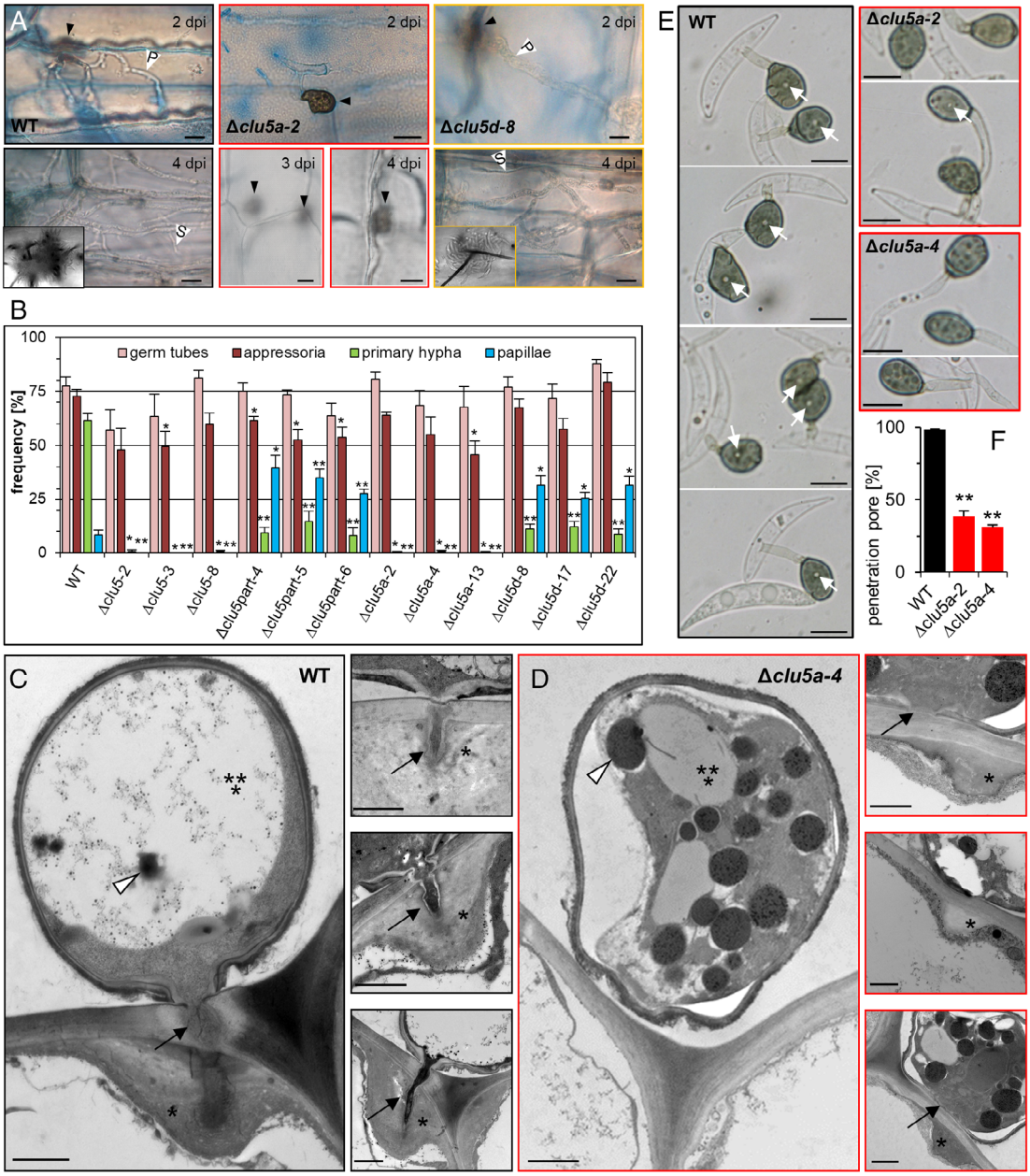

Fig. 4. Morphogenesis of *CLU5* mutants. A.–D. Leaves of *Z. mays* cv. Mikado were inoculated with 10^4 conidia per site, 14 days after sowing. A. Micrographs obtained by LM after staining with Aniline blue show fungal development in the epidermal layer at the indicated times. Focal plane is under the appressorium except for Δ*clu5a-2* at 2 dpi and the two insertions documenting early development of acervuli, which was not observed for the Δ*clu5a* mutant. Black arrowheads mark appressoria, P marks biotrophic primary hypha, S marks necrotrophic secondary hypha. Scale bars represent 10 μm. B. Quantitative assessments of fungal morphogenesis and papilla formation by the host at 3 dpi as observed by LM. Columns represent means of results from three infected leaves. In each replicate, infection structures advancing from 100 conidia and the resultant host responses were counted. Error bars provide SE, one asterisk indicates a significant difference between a mutant and the WT at $p < 0.05$, and two asterisks at $p < 0.005$ (unpaired *t*-test). Appressoria of the WT (C) and Δ*clu5a-4* (D), and cell wall appositions formed by maize as observed by TEM at 3 dpi. Large micrographs highlight representative appressoria, small micrographs papillae (asterisks). C. Most of the interior of the appressorium is occupied by a large vacuole (triple asterisk) with a few remaining dark lipid droplets inside (arrowhead), whereas the cytoplasm associating with the periphery of the cell is invading the penetration hypha (arrow, large image). Plant cells may form a papilla (asterisks) at the site of appressorium formation. Appressoria typically form a penetration hypha (arrows). D. Dark structures (arrowhead) supposedly containing lipids are visible in the cytoplasm of appressoria, some of them associated but not fused with vacuoles (triple asterisk). The contact of appressoria that do not form penetration hypha may induce small papillae (asterisks). Note the size difference to those formed by plant cells attacked by the WT. Scale bars in (C) and (D) represent 1 μm. E., F. Penetration pores in appressoria formed *in vitro*. Infection structures developed on plastic sheets in moistened petri dishes at RT in the dark for 48 hpi. E. Representative micrographs of WT, Δ*clu5a-2* and Δ*clu5a-4*. Arrows indicate penetration pores. Scale bars represent 10 μm. F. For each strain, 100 appressoria were observed by LM in each of six repetitions ($n = 6$; unpaired *t*-test, $p < 0.005$).

differentiated on plastic sheets, confirmed that the Δ*clu5a* mutants formed significantly fewer of these structures than the WT (Fig. 4E, F). Appressoria of these mutants often appeared indented (Fig. 4D), indicative of cell wall alterations, and contained several electron-dense spherical structures (Fig. 4D; arrowhead) likely representing lipid droplets (Schadeck *et al*., 1998; Weber *et al*., 2001). In the WT, these structures had almost vanished and a large central vacuole had appeared (Fig. 4C; triple asterisk). Appressoria were allowed to differentiate *in vitro* on glass slides and stained with Nile red. This dye stains intracellular lipid droplets as it binds to neutral triglycerides, and it can be detected by fluorescence microscopy (Greenspan and Fowler, 1985), allowing to investigate lipid dynamics (Wang *et al*., 2018). We observed a heterogeneous population of vesicles inside appressoria, several of which were stained by Nile red (Fig. S8). Previous studies have shown that apart from lipid vesicles, other types of spherical vesicles exist within appressoria and that Nile red does not stain all vesicles (Thines *et al*., 2000; Liu *et al*., 2007; Li *et al*., 2016; Wang *et al*., 2018). Remarkably, we did not observe notable differences between the mutants and the WT regarding size and number of Nile red-stained lipid vesicles suggesting that lipid reserves in appressoria were similar and distinct degradation rates were unlikely to cause the block in penetration in Δ*clu5a* mutants (Fig. S8). TEM further revealed that papillae were also formed in response to Δ*clu5a* mutants (Fig. 4D, inserts; asterisks), but these were much smaller and less electron-dense than those formed underneath WT appressoria (Fig. 4C, inserts; asterisks), explaining why they were not seen by LM.

Neither staining of *in vitro* differentiated infection structures with Calcofluor to label cell walls (Fig. S8), nor staining of infected maize leaves with diaminobenzidine (DAB) to visualize the formation of hydrogen peroxide (Fig. S9), detected notable differences between the WT and the mutants analysed.

The Δ*clu5d* mutants formed germ tubes and appressoria at rates similar to the WT, but their penetration rates were significantly reduced (Fig. 4B). In contrast to the Δ*clu5a* mutants, Δ*clu5d* mutants kept a residual penetration competence to form infection vesicles and voluminous biotrophic hyphae in the initially penetrated epidermal cells to spread to neighbouring cells and to form secondary hyphae (Figs. 4A, B; see also Fig. 2C). These mutants caused clearly weaker symptoms than the WT but induced papilla formation at significantly higher rates than the WT (Fig. 4B).

Δ*clu5a* mutants resembled mutants lacking the entire cluster, since the latter also failed to penetrate epidermal cells and to elicit papillae visible by LM (Fig. 4B, Fig. S10). On the other hand, Δ*clu5d* mutants resembled the Δ*clu5part* mutants carrying a deletion spanning *CLU5b* to *CLU5e* (Fig. 2A), since penetration and papilla formation rates were similar in these strains. These findings suggested that of the five genes analysed only *CLU5a* and *CLU5d* affect virulence.

Loss of appressorial penetration competence may result from reduced turgor pressure in these cells. Thus, we exposed Δ*clu5a* and Δ*clu5d* mutants to increasing concentrations of polyethylene glycol (PEG) 6000 (Howard *et al*., 1991). Intriguingly, Δ*clu5a* mutants displayed a significantly decreased frequency of cytorrhysis and an increase of a phenomenon called cavitation (Fig. 5A, right boxes, lower inserts, Fig. 5B, red lines). Cavitation was proposed to occur in fungal cells with walls sufficiently rigid to resist indenting or collapsing upon osmolyte-induced loss of water. Intense adhesion between the cytoplasmic membrane and the cell wall may cause also cavitation (Milburn, 1970; Money *et al*., 1998). The Δ*clu5d* mutants resembled the WT for both phenomena, i.e. cytorrhysis and cavitation. Deletion mutants of the remaining genes in cluster *CLU5* showed only marginal deviations from the WT.

PEG 200, glycol (=ethane-1,2-diol) and NaCl, which are osmolytes with smaller radii than PEG 6000, did not differentiate the mutants analysed from the WT for the phenomena of cytorrhysis, cavitation and plasmolysis (Fig. S11). Thus, the pore sizes of the cell wall are most likely not altered in the mutants. Scanning electron microscopy (SEM) and atomic force microscopy did neither reveal differences between the mutants and the WT with respect to surface topography and local elasticity of appressoria (Figs. S12 and S13).

To gain further insight into the function of Clu5a, the sequence of the mature protein served to generate *ab initio* 3D models. The model with the highest probability showed two hydrophobic patches at opposite surfaces of the peptide (Fig. 6A, green colour). The two cysteine residues at positions 23 and 33 of mature Clu5a located also at the surface of the model (cysteines as yellow stick model on ribbon in Fig. 6A).

This model was then used to analyse the nature of possible interaction partners using molecules as ligands residing in the fungal cell wall or the plasma membrane, or plant epicuticular wax. Interactions occurring on both sides of the Clu5a model were simulated for chitin, chitosan, schizophyllan, glycosylceramide as components of fungal cell walls or membranes, and 16,16-dihydroxyhexadecanoid acid (HXD) and octadeca-cis-6,cis-diene-1,18-dioate (OCD) as components of plant epicuticular wax. Testing all poses for a given Clu5a-ligand pair, those producing the highest scores were further analysed with molecular dynamic simulations to determine their binding free energies. This analysis indicated that positive charges such as present in chitosan are unlikely to interact with Clu5a, whereas hydrophobic

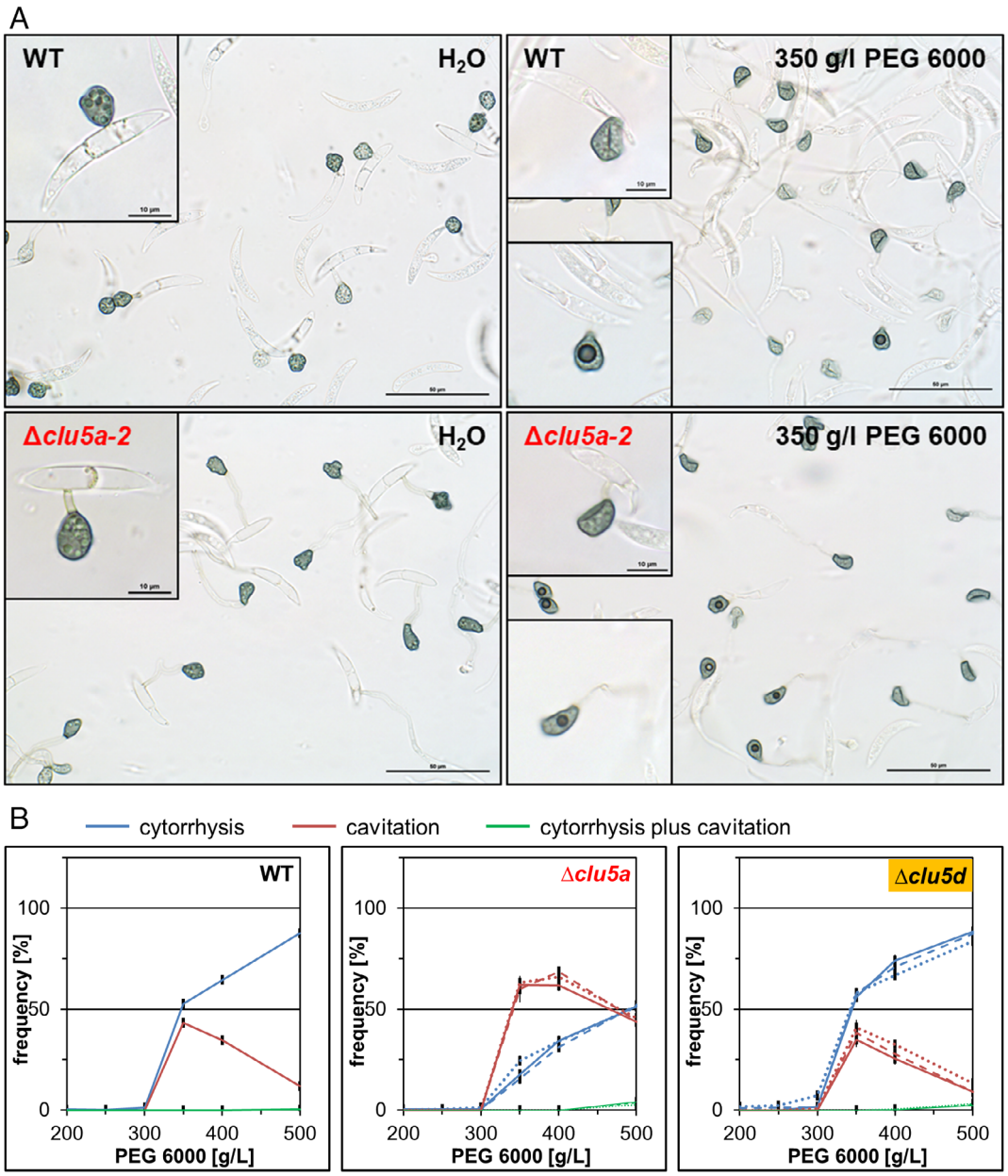

Fig. 5. Cytorrhysis and cavitation of appressoria. Infection structures of mutants and the WT developed on plastic sheets for 48 h before they were treated with PEG 6000. A. Micrographs obtained by LM of the WT and Δ*clu5a-2*. Insertions show characteristic appressoria exhibiting in the treated samples cell collapse, i.e. cytorrhysis (upper boxes) and cavitation (lower boxes). Bars represent 50 μm, resp. 10 μm (boxes). B. Series of PEG 6000 concentrations to quantify cytorrhysis and cavitation. Δ*clu5a*: dotted line represents clone Δ*clu5a-13*, broken line Δ*clu5a-4*, straight line Δ*clu5a-2*. Δ*clu5d*: dotted line represents clone Δ*clu5d-22*, broken line Δ*clu5d-17*, straight line Δ*clu5d-8*. Data represent means of six replicates, each assessing 100 appressoria (n = 6). Error bars show SE.

stretches such as in OCD and HXD are likely to be involved (Fig. 6B).

Since the predicted distance between the two cysteines in Clu5a was too large (18 Å) to allow for an intramolecular cysteine bridge (Fig. 6A) intermolecular disulphide bridges were analysed in 100 simulated homodimer complexes. Analysis of the distance between the sulphur atoms at Cys33 in both monomers retrieved a minimum of 13 Å among these complexes, which is too large to allow for a cysteine bridge. However, analysis of the distances between Cys23 in one monomer and Cys23 in the other yielded a minimum of 3.7 Å and for the Cys23-Cys33 paring of 4.7 Å. For both Cys pairings, rotation of the thiol groups along the Cα-Cβ axes reduced the distances between the respective sulphur atoms to about 2 Å, which is feasible for disulphide bridge formation

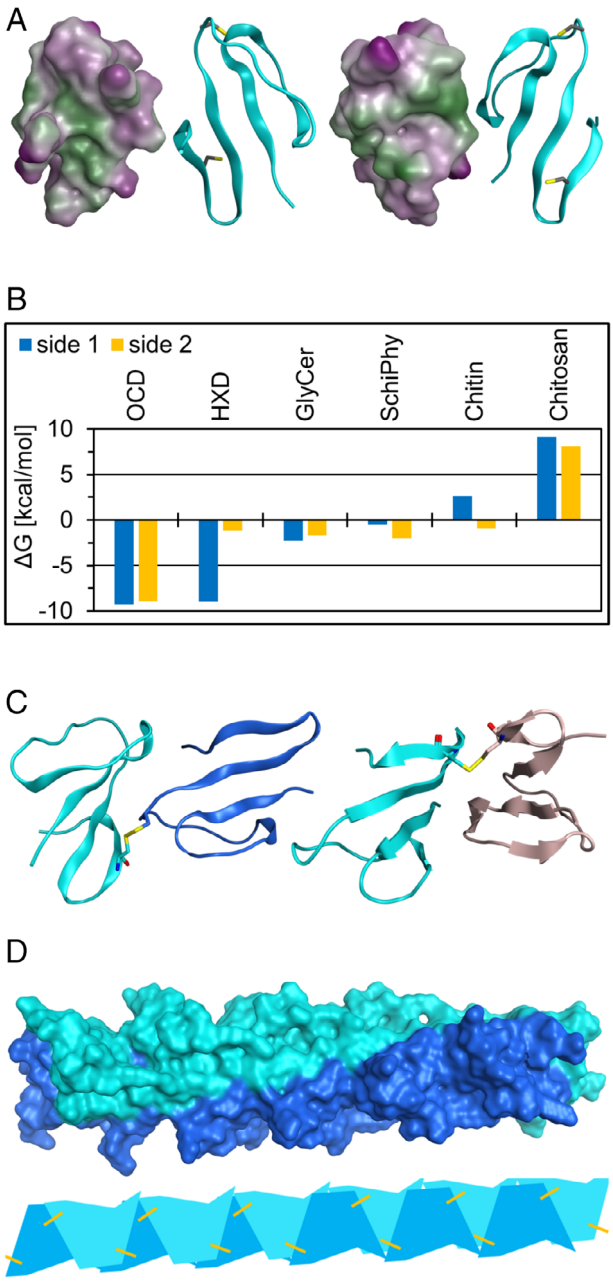

Fig. 6. Predicted structure of Clu5a. A. Protein model obtained by *ab initio* prediction by the Robetta server. The surface of the model shows areas with high lipophilicity in green and areas with high polarity in purple. The ribbon model shows the position of the cysteine residues (yellow). The first two models show the face, whereas the two models on the right show the back of Clu5a. B. Binding affinities of both sides of Clu5a with putative ligands determined by molecular dynamic simulations. Tested ligands are octadeca-cis-6,cis-diene-1,18-dioate (OCD), 16,16-dihydroxyhexadecanoid acid (HXD), glycosylceramide (GlyCer), schizophyllan (SchiPhy), chitin and chitosan. C. Ribbon models of Clu5a dimers with Cys23-Cys23 (left) and Cys23-Cys33 (right) disulphide bridges (yellow). D. Surface model of a Clu5a multimer (n = 12), consisting of repeated Cys23-Cys33 dimers, odd numbers in cyan, even numbers in blue, same as in a schematic model (each monomer represented by one polygon) with disulphide bridges (yellow).

(Fig. 6C, yellow sticks). Of functional importance, the dimer with a Cys23–Cys23 disulphide bridge (Fig. 6C, left model) has the ability to form a multimer (Fig. 6D) possibly hinting to a role in cell wall function.

Discussion

Recent studies have shown that secreted proteins are required for the establishment of compatible interactions between fungal pathogens with their host plants. In the present study, 58 genes of *C. graminicola*, encoding secreted candidate proteins were deleted, identifying two genes that are required for pathogenesis. Remarkably, these two genes, i.e. *CLU5a* and *CLU5d* residing in the same cluster of five co-linear genes, are important for appressorial penetration of intact host epidermal cells and for pathogenicity/virulence.

The present study indicates that of the proteins secreted by *C. graminicola*, only few are essential for fungal virulence, which is reminiscent of *M. oryzae*, where only 1 of 78 candidate proteins was involved in pathogenicity (Saitoh *et al*., 2012). About twice as many genes (18.6%) encoding secreted proteins, as compared with *C. graminicola* (according to the strict definition, see above), reside in clusters of up to 26 genes in the basidiomycete *Ustilago maydis*, with 5 of 12 clusters contributing to pathogenicity (Kämper *et al*., 2006). The clusters of *C. graminicola* are smaller and of those analysed only one contained genes with roles in the infection process. The paucity of detectable changes in pathogenicity of *C. graminicola* and *M. oryzae* after mutagenizing genes encoding secreted proteins does not necessarily indicate that such proteins are not involved in pathogenesis. Some of them may cause changes in virulence that are too small to allow for their detection in screens assessing symptoms, whereas other may be functionally redundant. Furthermore, the recent discovery of 'decoy effectors' that protect functional effectors from recognition by the host (Paulus *et al*., 2017) may further explain the paucity of candidate virulence proteins discovered in large screens in *M. oryzae* and *C. graminicola*.

It is striking that mature Clu5a is predicted to comprise only 38 aa. LM and TEM of infected leaves uncovered that Δ*clu5a* mutants formed germ tubes and appressoria on the surface of maize leaves at similar rates as the WT did but failed to penetrate the epidermal cell wall. This confirms a previous report on corresponding orthologues in *M. oryzae* and *C. orbiculare* that described Δ*mc69* mutants as penetration deficient (Saitoh *et al*., 2012; Irieda *et al*., 2014). The notion that 'MC69 is dispensable for appressorium formation' (Saitoh *et al*., 2012) is only partially supported by our TEM observations since appressoria formed by the Δ*clu5a* mutants had altered shapes and subcellular morphology. This is possibly due

to their inability to form the penetration peg causing the failure to invade the host.

Although a MoMC69::mCherry fusion protein localized at the biotrophic interfacial complex of *M. oryzae*, a structure delivering cytoplasmic effectors into host cells (Giraldo *et al*., 2013), translocation into rice cells was not detected (Saitoh *et al*., 2012). Furthermore, fluorescence-labelled CoMC69 located at a ring-like structure underneath the appressorium of *C. orbiculare*, suggesting that this protein accumulates in the interface between the penetration hypha and the invaded host cell. Again, translocation into host cells was not detected, leading to the view that MC69 is not a cytoplasmic effector (Irieda *et al*., 2014). As *MoMC69* (Saitoh *et al*., 2012), like *CLU5a* in *C. graminicola* and *C. higginsianum* (see Fig. S6), is transcribed throughout vegetative and pathogenic development and since this peptide has orthologues in saprophytes, one may question its effector function. Considering that Clu5a is an orthologue of the MC69 proteins, we suppose it may neither translocate into host cells. Beside a possible role as an apoplastic effector acting in the interface between fungal and host cells, Clu5a may localize in the fungal cell wall. Since Δ*clu5a* mutants formed penetration pores at significantly reduced rates and failed to develop penetration pegs, we hypothesise that this peptide may play a role in cell wall function, which is also suggested by our cytorrhysis experiments. Furthermore, the Δ*clu5a* mutants are impaired in spreading in wounded stalk tissues, which does not require appressoria. In contrast, these mutants are not impaired in spreading in wounded leaves. This apparent discrepancy may connect with the particular mode of pathogenesis in stalks, where *C. graminicola* hyphae grow rapidly along fibre cells in vascular bundles away from the site of inoculation to invade at a distance neighbouring parenchyma cells thereby starting secondary lesions (Tang *et al*., 2006; Venard and Vaillancourt, 2007). If Clu5a would play a role in fungal cell wall function, this role may extend beyond appressorial penetration, which would explain its occurrence even in saprophytes and the transcriptional patterns described above.

Application of osmolytes differing in molecular weight and radii did not induce plasmolysis in any strain tested, suggesting that the pore size of appressorial cell walls of Δ*clu5a* mutants is not altered. However, while the frequency of appressorial cytorrhysis decreased in the mutants, the cavitation rates increased after treatment with PEG 6000 suggesting a role of Clu5a in cell wall rigidity (Milburn, 1970; Money *et al*., 1998). The defect of the Δ*clu5a* mutants to form the penetration hypha could theoretically increase the turgor pressure far beyond levels reached in the WT, which eventually could lead to an appressorial burst, as observed in mutants of beta-1,3-glucan synthase (Oliveira-Garcia and Deising, 2013). This however did not happen. Strengthening of the appressorial cell wall and the cessation of lipid mobilization seem appropriate countermeasures to restrain turgor pressure. Notably, in *M. oryzae* differentiation of appressoria was shown to be a highly coordinated process involving the passage through two independent cell cycle checkpoints. Progression through the second checkpoint, which leads to the formation of the penetration hypha, seems to be controlled by a turgor threshold (Oses-Ruiz *et al*., 2017). Possibly, a similar mechanism may exist in *C. graminicola* that prevents appressorial burst in the Δ*clu5a* mutants.

The predicted 3D structure of Clu5a indicates that two Cys residues may form a disulphide bridge between two Clu5a monomers, yielding a dimer, possibly extending to multimerization. Remarkably, the alignment of Clu5a peptides reveals that seven amino acids are strictly conserved in all species analysed (Fig. S7). Among those are Cys23 and Cys33 in Clu5a. In *M. oryzae*, the corresponding amino acids are thought to form a disulphide bridge since these residues are essential to preserve the function of MC69 in pathogenicity (Saitoh *et al*., 2012). Our 3D model contrasts this hypothesis and indicates that the two Cys are too far apart to form an intramolecular disulphide bridge but instead may form intermolecular bridges. Therefore, Clu5a may form dimers or multimers.

Besides fungal morphogenesis, we detected further differences between the Δ*clu5a* mutants and the WT in triggering of host defence. In most instances, the WT strain of *C. graminicola* breaches mature papillae in case they are formed, thus permitting further ingress (Mims and Vaillancourt, 2002; Weihmann *et al*., 2016). The Δ*clu5a* mutants, however, elicit small papillae only evidenced by TEM, suggesting that appressoria of these mutants may not be able to initiate infection peg development and induce ineffective initials of papillae only. Fortification of these initials, for instance, by the apposition of callose or incrustation with lignin, may only occur after the penetration hypha emerges from the appressorium. Thus, appressoria formed by the Δ*clu5a* mutants are recognized by maize epidermal cells, but they elicit a weaker papilla response than the WT, and possibly due to altered cell wall rigidity, leading to arrested infection-related development and, hence, reduced PAMP exposure.

Within *CLU5*, we identified a second conserved gene, *CLU5d*, the deletion of which caused diminished virulence. *CLU5d* had previously been identified by YSST (Krijger *et al*., 2008), indicating that Clu5d is a secreted protein. Like Clu5a, Clu5d does not have amino acid sequence features allowing to predict its function. LM of infected leaves showed that Δ*clu5d* mutants penetrate intact leaf surfaces at significantly reduced rates and induced significantly more papillae than the WT. However, this response

is insufficient to prevent completely further ingress. Interestingly, *CLU5d* belongs to the core of the cluster since it exists at a consistent position and orientation in all species of the Sordariomycetes analysed. Appressorial penetration incompetence observed in both Δ*clu5a* and Δ*clu5d* mutants suggests participation of the proteins in the same cellular function or pathway, with the former being epistatic to the latter protein. In this case, potential effects of the deletion of *CLU5d* would be masked in the deletion comprising the entire cluster. Since the individual deletions of the remaining three genes analysed in this study and since the phenotypes seen in the Δ*clu5part* and the Δ*clu5d* mutants were comparable, as were the phenotypes of the Δ*clu5* and the Δ*clu5a* mutants, we conclude that *CLU5b*, *CLU5c* and *CLU5e* are not essential for pathogenicity of *C. graminicola* in maize leaves and stalks.

In conclusion, a large screen in *C. graminicola* led to the discovery of two virulence factors encoded by genes residing in a gene cluster for secreted proteins. Intriguingly, Clu5a is essential for appressorial penetration and, as a consequence, for pathogenicity. We hypothesise that it may have roles in modulating cell wall properties critical for appressorial penetration of the host epidermis. Because of the expression of the *CLU* genes during all developmental phases, including vegetative growth, the conservation of synteny and the occurrence of orthologues in both pathogenic and non-pathogenic fungi, we suppose that *CLU5a* and *CLU5d* play important roles in fungal biology that extend beyond their involvement in appressorial penetration.

Experimental procedures

Cultivation of fungi and plants

As WT reference, strain M1.001 of *Colletotrichum graminicola* (Ces.) Wilson (teleomorph *Glomerella graminicola* (Politis)) was used (Vaillancourt and Hanau, 1991). Mutants used in this study are described below. Vegetative growth, conidiation and germination assays were done as described (Oliveira-Garcia and Deising, 2013).

Plants used for inoculation included maize cultivars Mikado (KWS Saat AG, Einbeck, Germany), B73 (ARS-USDA, Ames, Iowa, USA), Farmtop (FarmSaat AG, Everswinkel, Germany) and Golden Jubilee (Territorial Seed Company, Cottage Grove, OR). Plants grew in the greenhouse and in environmentally controlled growth chambers as described (Behr *et al*., 2010; Abou Ammar *et al*., 2013).

Generation of mutants

Candidate genes were deleted by transforming protoplasts as described (Werner *et al*., 2007). Linear PCR constructs used for transformation were generated according to the DJ-PCR procedure (Yu *et al*., 2004). Oligonucleotides used for the constructions are provided in Table S1. Analysis of transformants by PCR and Southern hybridization was performed as reported (Horbach *et al*., 2009; Oliveira-Garcia and Deising, 2013).

Deletion mutants chosen for complementation were co-transformed with the respective WT allele surrounded by about 1 kb of flanking DNA that was obtained by PCR. In addition, pAN7-1 was included in the transformation reaction to allow for selection of hygromycin-resistant transformants.

Virulence assays

Virulence of *C. graminicola* strains was assayed employing detached maize leaves (Horbach *et al*., 2009; Oliveira-Garcia and Deising, 2013). In addition, a quantitative stalk infection assay was used (Abou Ammar *et al*., 2013). For the latter, 10,000 falcate conidia suspended in 10 μl of 0.02% Tween 20 were pipetted into a small cavity made at the first internode of stalks of 6-week-old maize cultivar Mikado plants. Necrotic areas in longitudinally split stalks were measured at 14 dpi, using the computer program ImageJ version 1.46.

qPCR

Except for minor modifications, we followed published procedures to determine the amount of *C. graminicola* DNA in infected maize cv. Mikado (Weihmann *et al*., 2016). For each strain analysed, we inoculated the middle sections of three leaves with four droplets each containing 1×10^4 conidia. Harvesting was done at 4 dpi by combining the four excised infection sites of each leaf to represent one repetition.

Assessment of appressorial turgor pressure and cell wall properties

Treatment with PEG served to assess turgor pressure (Howard *et al*., 1991). A suspension of 10 ml of falcate conidia, which were freshly harvested from an OMA plate and adjusted to 4×10^6 ml^{-1}, was distributed onto a plastic sheet (plain paper copier film, ACCO Brand, Aylesbury, UK) fitted to a petri dish of 5.5 cm diameter. Excessive liquid was discarded after an incubation of 1 h at RT. A moistened filter paper in the lid of the petri dish and parafilm provided high moisture for fungal differentiation, which occurred in the dark at 23°C for 24 h. The plastic sheet was then transferred successively to petri dishes containing 15 ml of H_2O for a gentle wash and PEG 6000 of the chosen concentration, where it was incubated for 15 min at RT. This osmolyte cannot pass the appressorial cell wall thus leading at a sufficiently

high concentration to a collapse of the structure (cytorrhysis), which was observed by bright field microscopy. Treatment with PEG 6000 also caused the phenomenon of cavitation, i.e. the occurrence of a gas bubble within the cytoplasm (Milburn, 1970; Money *et al*., 1998). The porosity of the appressorial cell wall was assessed by treatment with other smaller osmolytes of various molecular weights. Osmolytes able to permeate the cell wall but not the plasma membrane will induce the detachment of the latter from the former (plasmolysis).

Topographical and mechanical data of appressorial surfaces were obtained by atomic force microscope NanoWizard II (JPK-Instruments, Berlin) using Force-Spectroscopy mode. Appressoria analysed had differentiated on cover slips from falcate conidia that were inoculated as above. Analysis was performed at RT in a closed liquid cell (JPK-Instruments, Berlin). A MLCT-cantilever (Bruker, USA) was used with a tip radius of approximately 50 nm verified before and after experimentation by Scanning Electron Microscopy Quanta 3D (FEI, USA). A spring constant of 0.1 N m^{-1} $\pm$ 0.02 was determined using the thermal noise method (Sader *et al*., 1999). For each appressorium analysed, more than 16,000 data points were obtained in a grid map of 2 $\times$ 2 μm^2 with equal distances of 16 nm in *x*- and *y*-directions to acquire topographical micrographs as well as information on local elasticity. Young's modulus was determined from the force-indentation curve according to an advanced Hertzian model for spherical indenter geometry (Johnson, 1985).

Microscopy

Bright field and fluorescence microscopy including stains using DAB, Aniline blue and Calcofluor white were performed as reported (Oliveira-Garcia and Deising, 2013; Weihmann *et al*., 2016). Nile red was used to stain lipid droplets as published (Ludwig *et al*., 2014). TEM used leaf discs that were fixed for 4 h with 3% glutaraldehyde (Sigma, Taufkirchen, Germany) in 0.1 M sodium cacodylate buffer pH 7.2 (SCB), washed, post-fixed for 1 h with 1% osmium tetroxide (Carl Roth, Karlsruhe, Germany) in SCB, dehydrated in a graded series of ethanol and embedded in epoxy resin (Spurr, 1969). Ultrathin sections (70 nm) were transferred to formvar-coated grids and post-stained with uranyl acetate and lead citrate. Afterwards, the grids were observed with a LIBRA 120 (Carl Zeiss Microscopy, Oberkochen, Germany) transmission electron microscope (acceleration voltage 120 kV). Electron micrographs were taken with a dual-speed on axis SSCCD camera (BM-2 k-120; TRS, Moorenweis, Germany) using the iTEM software (Olympus SIS, Münster, Germany). Highly resolved views of appressorial surfaces were obtained by a Dual Beam Scanning Electron Microscope Quanta 3D (FEI; Hillsboro, OR, USA) at 5 kV using secondary electron detectors. Appressoria analysed had differentiated on cover slips from falcate conidia that were inoculated as above. Sample preparation for SEM followed established protocols for fixation, staining, dehydration and sputtering conductive coating (Karnovsky, 1965; Nation, 1983; Glauert, 1984).

Bioinformatics

Using the annotated proteome of *C. graminicola* strain M1.001 (O'Connell *et al*., 2012), the encoded secretome was predicted *de novo* using the computer programs SignalP 2.0, Signal P 3.0 and TargetP (all on http://www.cbs.dtu.dk/services/). As proposed earlier (Klee and Ellis, 2005), proteins were only regarded as secreted when all three programs predicted this. Transmembrane domains were identified using the program Phobius (http://phobius.sbc.su.se/) (Käll *et al*., 2005). Programs used for the prediction of the subcellular localisation of proteins were Wolf PSort (http://www.genscript.com/psort/wolf_psort.html) (Horton *et al*., 2007) and PredictProtein (http://www.predictprotein.org/) (Yachdav *et al*., 2014). The program Augustus (http://bioinf.uni-greifswald.de/augustus/) was applied for gene predictions.

Similarity searches for DNA and protein sequences used the Blast suite of programs with default parameters (http://blast.ncbi.nlm.nih.gov/Blast.cgi). Phylogenetic analysis employed the software MEGA version 6 (http://www.megasoftware.net/) (Tamura *et al*., 2013). Maximum Likelihood (ML) trees were estimated applying the best model computed by the program. All positions with less than 90% site coverage were eliminated. That is, fewer than 10% alignment gaps, missing data, and ambiguous bases were allowed at any position. Initial trees for the heuristic search were obtained automatically by applying Neighbor-Join and BioNJ algorithms to a matrix of pairwise distances estimated using a JTT model, and then selecting the topology with superior log likelihood value. Obtained ML trees were evaluated by 1000 bootstrap replicates.

CLU5 is located on chromosome 8 neither close to a telomere nor to the centromere (see Fig. 1). To analyse conservation of synteny, orthologues of *CLU5a* to *CLU5e* and genes flanking them (GLRG_04684 to GLRG_04691) were identified by BlastP using the annotated protein sequences as queries against the annotated proteins of *C. sublineola* TX430BB (Baroncelli *et al*., 2014), *C. higginsianum* IMI 349063 (Zampounis *et al*., 2016), *C. incanum* MAFF 238704 (Hacquard *et al*., 2016), *C. tofieldiae* 0861 (Hacquard *et al*., 2016), *C. chlorophyti* NTL11 (Gan *et al*., 2017), *C. orchidophilum* IMI 309357 (Baroncelli *et al*., 2018), *C. nymphaeae* IMI 504889 (Baroncelli *et al*., 2016),

C. simmondsii CBS 122122 (Baroncelli *et al*., 2016), *C. fioriniae* IMI 504882 (Baroncelli *et al*., 2016), *C. salicis* CBS 607.94 (Baroncelli *et al*., 2016), *C. fruticola* nara gc5 (Gan *et al*., 2013), *C. gloeosporioides* Cg-14 (Alkan *et al*., 2013), *C. orbiculare* MAFF 240422 (Gan *et al*., 2013), *V. dahliae* (Faino *et al*., 2015), *F. graminearum* (King *et al*., 2017), *M. oryzae* 70–15 (Dean *et al*., 2005), *B. bassiana* ARSEF 8028 (Valero-Jimenez *et al*., 2016), *C. militaris* CM01 (Kramer and Nodwell, 2017), *C. thermophilum* DSM 1495 (Bock *et al*., 2014), *N. crassa* 74-OR23-1A (Galagan *et al*., 2003) and *T. harzianum* CBS 226.95 (Steindorff *et al*., 2014). BlastP searches yielding no hits were repeated using TblastN.

The protein sequence of Clu5a was used to model its 3D structure by the Robetta server using the Rosetta *de novo* protocol (Raman *et al*., 2009). The received models (A–E) were evaluated based on their stereochemistry and similarity to native folds (Wiederstein and Sippl, 2007). Regarding outliers of phi/psi dihedrals, of C-beta dihedrals, of omega dihedrals, of bond lengths and angles, models A and E performed best (no outliers) as analysed by the computer program MOE 2016.08 (https://www.chemcomp.com/MOE-Molecular_Operating_Environment.htm). Regarding the ProSA z-score, all models showed native like folds, with models A and D being closest to the medium value. Because model A performed best in both tests, it was chosen for further analysis. The calculations of the protein surface, plotting of lipophilicity on it and protein–protein-docking have been performed using the program MOE 2016.08. Complexes were selected when an intermolecular bisulfide bridge was possible. The program GOLD v5.2.2 with the scoring function CHEMPLP positioned putative ligands on the surface of the Clu5a model (Jones *et al*., 1997; Korb *et al*., 2009).The binding-free energies of the generated protein–ligand complexes were calculated using Linear Interaction Energies with $\beta = 0.06$ und $\alpha = 0.18$ (Almlöf *et al*., 2007). Therefore, molecular dynamic simulations have been run using NAMD 2.12 with NpT ensemble at 300 K for 1 ns and CHARMM36 force field parameters. The ligand's parameters were generated by CGenFF (Phillips *et al*., 2005; Vanommeslaeghe *et al*., 2012; Vanommeslaeghe and MacKerell, 2012). Visualization and analysis of MDS have been done with VMD 1.94 and the NAMDEnergy plug in V1.4 (Humphrey *et al*., 1996).

Acknowledgements

We thank Diana Gottschling, Lydia Krasper for technical assistance and Elke Vollmer for greenhouse services. We gratefully acknowledge Ralf Horbach, Ely Oliveira-Garcia and Ivo Schliebner who supported us during different phases of the project with materials.

This study was supported by a DFG-grant provided in the framework of the SFB 648 (project A5) and by a grant from the federal state of Saxony-Anhalt provided through the Interdisciplinary Centre for Crop Plant Research (Interdisziplinäres Zentrum für Nutzpflanzenforschung, IZN, project 08).

References

Abou Ammar, G., Tryono, R., Döll, K., Karlovsky, P., Deising, H.B., and Wirsel, S.G.R. (2013) Identification of ABC transporter genes of *Fusarium graminearum* with roles in azole tolerance and/or virulence. *PLoS One* **8**: e79042.

Albarouki, E., Schafferer, L., Ye, F., von Wiren, N., Haas, H., and Deising, H.B. (2014) Biotrophy-specific down-regulation of siderophore biosynthesis in *Colletotrichum graminicola* is required for modulation of immune responses of maize. *Mol Microbiol* **92**: 338–355.

Alkan, N., Meng, X., Friedlander, G., Reuveni, E., Sukno, S., Sherman, A., *et al*. (2013) Global aspects of pacC regulation of pathogenicity genes in *Colletotrichum gloeosporioides* as revealed by transcriptome analysis. *Mol Plant Microbe Interact* **26**: 1345–1358.

Almlöf, M., Carlsson, J., and Aqvist, J. (2007) Improving the accuracy of the linear interaction energy method for solvation free energies. *J Chem Theory Comput* **3**: 2162–2175.

Baroncelli, R., Sanz-Martin, J.M., Rech, G.E., Sukno, S.A., and Thon, M.R. (2014) Draft genome sequence of *Colletotrichum sublineola*, a destructive pathogen of cultivated *Sorghum*. *Genome Announc* **2**: e00540–e00514.

Baroncelli, R., Amby, D.B., Zapparata, A., Sarrocco, S., Vannacci, G., Le Floch, G., *et al*. (2016) Gene family expansions and contractions are associated with host range in plant pathogens of the genus *Colletotrichum*. *BMC Genomics* **17**: 555.

Baroncelli, R., Sukno, S.A., Sarrocco, S., Cafa, G., Le Floch, G., and Thon, M.R. (2018) Whole-genome sequence of the orchid anthracnose pathogen *Colletotrichum orchidophilum*. *Mol Plant Microbe Interact* **31**: 979–981.

Behr, M., Humbeck, K., Hause, G., Deising, H.B., and Wirsel, S.G.R. (2010) The hemibiotroph *Colletotrichum graminicola* locally induces photosynthetically active green islands but globally accelerates senescence on aging maize leaves. *Mol Plant Microbe Interact* **23**: 879–892.

Bergstrom, G.C., and Nicholson, R.L. (1999) The biology of corn anthracnose—knowledge to exploit for improved management. *Plant Dis* **83**: 596–608.

Bock, T., Chen, W.H., Ori, A., Malik, N., Silva-Martin, N., Huerta-Cepas, J., *et al*. (2014) An integrated approach for genome annotation of the eukaryotic thermophile *Chaetomium thermophilum*. *Nucleic Acids Res* **42**: 13525–13533.

da Costa, R.V., Cota, L.V., da Silva, D.D., Parreira, D.F., Casela, C.R., Landau, E.C., and Figueiredo, J.E.F. (2014) Races of *Colletotrichum graminicola* pathogenic to maize in Brazil. *Crop Prot* **56**: 44–49.

Dean, R.A., Talbot, N.J., Ebbole, D.J., Farman, M.L., Mitchell, T.K., Orbach, M.J., *et al*. (2005) The genome

sequence of the rice blast fungus *Magnaporthe grisea*. *Nature* **434**: 980–986.
El Gueddari, N.E., Rauchhaus, U., Moerschbacher, B.M., and Deising, H.B. (2002) Developmentally regulated conversion of surface-exposed chitin to chitosan in cell walls of plant pathogenic fungi. *New Phytol* **156**: 103–112.
Faino, L., Seidl, M.F., Datema, E., van den Berg, G.C., Janssen, A., Wittenberg, A.H., and Thomma, B.P. (2015) Single-molecule real-time sequencing combined with optical mapping yields completely finished fungal genome. *MBio* **6**: e00936–e00915.
Flor, H.H. (1971) Current status of gene-for-gene concept. *Annu Rev Phytopathol* **9**: 275–296.
Galagan, J.E., Calvo, S.E., Borkovich, K.A., Selker, E.U., Read, N.D., Jaffe, D., *et al*. (2003) The genome sequence of the filamentous fungus *Neurospora crassa*. *Nature* **422**: 859–868.
Gan, P., Ikeda, K., Irieda, H., Narusaka, M., O'Connell, R.J., Narusaka, Y., *et al*. (2013) Comparative genomic and transcriptomic analyses reveal the hemibiotrophic stage shift of *Colletotrichum* fungi. *New Phytol* **197**: 1236–1249.
Gan, P., Narusaka, M., Kumakura, N., Tsushima, A., Takano, Y., Narusaka, Y., and Shirasu, K. (2016) Genus-wide comparative genome analyses of *Colletotrichum* species reveal specific gene family losses and gains during adaptation to specific infection lifestyles. *Genome Biol Evol* **8**: 1467–1481.
Gan, P., Narusaka, M., Tsushima, A., Narusaka, Y., Takano, Y., and Shirasu, K. (2017) Draft genome assembly of *Colletotrichum chlorophyti*, a pathogen of herbaceous plants. *Genome Announc* **5**: e01733-01716.
Giraldo, M.C., Dagdas, Y.F., Gupta, Y.K., Mentlak, T.A., Yi, M., Martinez-Rocha, A.L., *et al*. (2013) Two distinct secretion systems facilitate tissue invasion by the rice blast fungus *Magnaporthe oryzae*. *Nat Commun* **4**: 1996.
Glauert, A.M. (ed). (1984) *Fixation, Dehydration and Embedding of Biological Specimens*. Amsterdam, Netherlands: Elsevier.
Greenspan, P., and Fowler, S.D. (1985) Spectrofluorometric studies of the lipid probe nile red. *J Lipid Res* **26**: 781–789.
Hacquard, S., Kracher, B., Hiruma, K., Münch, P.C., Garrido-Oter, R., Thon, M.R., *et al*. (2016) Survival trade-offs in plant roots during colonization by closely related beneficial and pathogenic fungi. *Nat Commun* **7**: 11362.
Horbach, R., Graf, A., Weihmann, F., Antelo, L., Mathea, S., Liermann, J.C., *et al*. (2009) Sfp-type 4′-phosphopantetheinyl transferase is indispensable for fungal pathogenicity. *Plant Cell* **21**: 3379–3396.
Horton, P., Park, K.J., Obayashi, T., Fujita, N., Harada, H., Adams-Collier, C.J., and Nakai, K. (2007) WoLF PSORT: protein localization predictor. *Nucleic Acids Res* **35**: W585–W587.
Howard, R.J., Ferrari, M.A., Roach, D.H., and Money, N.P. (1991) Penetration of hard substrates by a fungus employing enormous turgor pressures. *Proc Natl Acad Sci U S A* **88**: 11281–11284.
Humphrey, W., Dalke, A., and Schulten, K. (1996) VMD: visual molecular dynamics. *J Mol Graph* **14**: 33–38.
Irieda, H., Maeda, H., Akiyama, K., Hagiwara, A., Saitoh, H., Uemura, A., *et al*. (2014) *Colletotrichum orbiculare* secretes virulence effectors to a biotrophic interface at the primary hyphal neck via exocytosis coupled with SEC22-mediated traffic. *Plant Cell* **26**: 2265–2281.
Jeon, J., Park, S.Y., Chi, M.H., Choi, J., Park, J., Rho, H.S., *et al*. (2007) Genome-wide functional analysis of pathogenicity genes in the rice blast fungus. *Nat Genet* **39**: 561–565.
Johnson, K.L. (1985) *Contact Mechanics*. Cambridge, UK: Cambridge University Press.
Jones, J.D.G., and Dangl, J.L. (2006) The plant immune system. *Nature* **444**: 323–329.
Jones, G., Willett, P., Glen, R.C., Leach, A.R., and Taylor, R. (1997) Development and validation of a genetic algorithm for flexible docking. *J Mol Biol* **267**: 727–748.
Käll, L., Krogh, A., and Sonnhammer, E.L.L. (2005) An HMM posterior decoder for sequence feature prediction that includes homology information. *Bioinformatics* **21**: I251–I257.
Kämper, J., Kahmann, R., Bölker, M., Ma, L.J., Brefort, T., Saville, B.J., *et al*. (2006) Insights from the genome of the biotrophic fungal plant pathogen *Ustilago maydis*. *Nature* **444**: 97–101.
Karnovsky, M.J. (1965) A formaldehyde-glutaraldehyde fixative of high osmolality for use in electron microscopy. *J Cell Biol* **27**: 137.
King, R., Urban, M., and Hammond-Kosack, K.E. (2017) Annotation of *Fusarium graminearum* (PH-1) version 5.0. *Genome Announc* **5**: e01479–e01416.
Klee, E.W., and Ellis, L.B.M. (2005) Evaluating eukaryotic secreted protein prediction. *BMC Bioinformatics* **6**: 256.
Korb, O., Stutzle, T., and Exner, T.E. (2009) Empirical scoring functions for advanced protein-ligand docking with PLANTS. *J Chem Inf Model* **49**: 84–96.
Kramer, G.J., and Nodwell, J.R. (2017) Chromosome level assembly and secondary metabolite potential of the parasitic fungus *Cordyceps militaris*. *BMC Genomics* **18**: 912.
Krijger, J.-J., Horbach, R., Behr, M., Schweizer, P., Deising, H.B., and Wirsel, S.G.R. (2008) The yeast signal sequence trap identifies secreted proteins of the hemibiotrophic corn pathogen *Colletotrichum graminicola*. *Mol Plant Microbe Interact* **21**: 1325–1336.
Li, Y., Zhu, J.D., Hu, J.X., Meng, X.L., Zhang, Q., Zhu, K.P., *et al*. (2016) Functional characterization of electron-transferring flavoprotein and its dehydrogenase required for fungal development and plant infection by the rice blast fungus. *Sci Rep* **6**: 24911.
Liu, X.H., Lu, J.P., Zhang, L., Dong, B., Min, H., and Lin, F. C. (2007) Involvement of a *Magnaporthe grisea* serine/threonine kinase gene, *MgATG1*, in appressorium turgor and pathogenesis. *Eukaryot Cell* **6**: 997–1005.
Lochman, J., and Mikes, V. (2006) Ergosterol treatment leads to the expression of a specific set of defence-related genes in tobacco. *Plant Mol Biol* **62**: 43–51.
Ludwig, N., Löhrer, M., Hempel, M., Mathea, S., Schliebner, I., Menzel, M., *et al*. (2014) Melanin is not required for turgor generation but enhances cell-wall rigidity in appressoria of the corn pathogen *Colletotrichum graminicola*. *Mol Plant Microbe Interact* **27**: 315–327.
Milburn, J.A. (1970) Cavitation and osmotic potentials of *Sordaria* ascospores. *New Phytol* **69**: 133–141.
Mims, C.W., and Vaillancourt, L.J. (2002) Ultrastructural characterization of infection and colonization of maize

leaves by *Colletotrichum graminicola*, and by a *C. graminicola* pathogenicity mutant. *Phytopathology* **92**: 803–812.

Money, N.P., Caesar-TonThat, T.C., Frederick, B., and Henson, J.M. (1998) Melanin synthesis is associated with changes in hyphopodial turgor, permeability, and wall rigidity in *Gaeumannomyces graminis* var. *graminis*. *Fungal Genet Biol* **24**: 240–251.

Nation, J.L. (1983) A new method using hexamethyldisilazane for preparation of soft insect tissues for scanning electron-microscopy. *Stain Technol* **58**: 347–351.

Newman, M.A., Sundelin, T., Nielsen, J.T., and Erbs, G. (2013) MAMP (microbe-associated molecular pattern) triggered immunity in plants. *Front Plant Sci* **4**: 139.

Nicholson, R.L., and Warren, H.L. (1976) Criteria for evaluation of resistance to maize anthracnose. *Phytopathology* **66**: 86–90.

O'Connell, R.J., Thon, M.R., Hacquard, S., Amyotte, S.G., Kleemann, J., Torres, M.F., *et al*. (2012) Lifestyle transitions in plant pathogenic *Colletotrichum* fungi deciphered by genome and transcriptome analyses. *Nat Genet* **44**: 1060–1065.

Oliveira-Garcia, E., and Deising, H.B. (2013) Infection structure-specific expression of beta-1,3-glucan synthase is essential for pathogenicity of *Colletotrichum graminicola* and evasion of beta-glucan-triggered immunity in maize. *Plant Cell* **25**: 2356–2378.

Oliveira-Garcia, E., and Deising, H.B. (2016) Attenuation of PAMP-triggered immunity in maize requires down-regulation of the key beta-1,6-glucan synthesis genes *KRE5* and *KRE6* in biotrophic hyphae of *Colletotrichum graminicola*. *Plant J* **87**: 355–375.

Oliveira-Garcia, E., and Valent, B. (2015) How eukaryotic filamentous pathogens evade plant recognition. *Curr Opin Microbiol* **26**: 92–101.

Oses-Ruiz, M., Sakulkoo, W., Littlejohn, G.R., Martin-Urdiroz, M., and Talbot, N.J. (2017) Two independent S-phase checkpoints regulate appressorium-mediated plant infection by the rice blast fungus *Magnaporthe oryzae*. *Proc Natl Acad Sci U S A* **114**: E237–E244.

Paulus, J.K., Kourelis, J., and van der Hoorn, R.A.L. (2017) Bodyguards: pathogen-derived decoys that protect virulence factors. *Trends Plant Sci* **22**: 355–357.

Phillips, J.C., Braun, R., Wang, W., Gumbart, J., Tajkhorshid, E., Villa, E., *et al*. (2005) Scalable molecular dynamics with NAMD. *J Comput Chem* **26**: 1781–1802.

Raman, S., Vernon, R., Thompson, J., Tyka, M., Sadreyev, R., Pei, J.M., *et al*. (2009) Structure prediction for CASP8 with all-atom refinement using Rosetta. *Proteins* **77**: 89–99.

Ravensdale, M., Nemri, A., Thrall, P.H., Ellis, J.G., and Dodds, P.N. (2011) Co-evolutionary interactions between host resistance and pathogen effector genes in flax rust disease. *Mol Plant Pathol* **12**: 93–102.

Sader, J.E., Chon, J.W.M., and Mulvaney, P. (1999) Calibration of rectangular atomic force microscope cantilevers. *Rev Sci Instrum* **70**: 3967–3969.

Saitoh, H., Fujisawa, S., Mitsuoka, C., Ito, A., Hirabuchi, A., Ikeda, K., *et al*. (2012) Large-scale gene disruption in *Magnaporthe oryzae* identifies MC69, a secreted protein required for infection by monocot and dicot fungal pathogens. *PLoS Pathog* **8**: e1002711.

Sanz-Martin, J.M., Pacheco-Arjona, J.R., Bello-Rico, V., Vargas, W.A., Monod, M., Diaz-Minguez, J.M., *et al*. (2016) A highly conserved metalloprotease effector enhances virulence in the maize anthracnose fungus *Colletotrichum graminicola*. *Mol Plant Pathol* **17**: 1048–1062.

Schadeck, R.J.G., Leite, B., and de Freitas Buchi, D. (1998) Lipid mobilization and acid phosphatase activity in lytic compartments during conidium dormancy and appressorium formation of *Colletotrichum graminicola*. *Cell Struct Funct* **23**: 333–340.

Schliebner, I., Becher, R., Hempel, M., Deising, H.B., and Horbach, R. (2014) New gene models and alternative splicing in the maize pathogen *Colletotrichum graminicola* revealed by RNA-Seq analysis. *BMC Genomics* **15**: 842.

Shetty, N.P., Jensen, J.D., Knudsen, A., Finnie, C., Geshi, N., Blennow, A., *et al*. (2009) Effects of beta-1,-3-glucan from *Septoria tritici* on structural defence responses in wheat. *J Exp Bot* **60**: 4287–4300.

Spurr, A.R. (1969) A low-viscosity epoxy resin embedding medium for electron microscopy. *J Ultrastruct Res* **26**: 31–43.

Steindorff, A.S., Ramada, M.H., Coelho, A.S., Miller, R.N., Pappas, G.J., Jr., Ulhoa, C.J., and Noronha, E.F. (2014) Identification of mycoparasitism-related genes against the phytopathogen *Sclerotinia sclerotiorum* through transcriptome and expression profile analysis in *Trichoderma harzianum*. *BMC Genomics* **15**: 204.

Tamura, K., Stecher, G., Peterson, D., Filipski, A., and Kumar, S. (2013) MEGA6: molecular evolutionary genetics analysis version 6.0. *Mol Biol Evol* **30**: 2725–2729.

Tang, W.H., Coughlan, S., Crane, E., Beatty, M., and Duvick, J. (2006) The application of laser microdissection to in planta gene expression profiling of the maize anthracnose stalk rot fungus *Colletotrichum graminicola*. *Mol Plant Microbe Interact* **19**: 1240–1250.

Thines, E., Weber, R.W.S., and Talbot, N.J. (2000) MAP kinase and protein kinase A-dependent mobilization of triacylglycerol and glycogen during appressorium turgor generation by *Magnaporthe grisea*. *Plant Cell* **12**: 1703–1718.

Torres, M.F., Ghaffari, N., Buiate, E.A., Moore, N., Schwartz, S., Johnson, C.D., and Vaillancourt, L.J. (2016) A *Colletotrichum graminicola* mutant deficient in the establishment of biotrophy reveals early transcriptional events in the maize anthracnose disease interaction. *BMC Genomics* **17**: 202.

Vaillancourt, L.J., and Hanau, R.M. (1991) A method for genetic analysis of *Glomerella graminicola* (*Colletotrichum graminicola*) from maize. *Phytopathology* **81**: 530–534.

Valero-Jimenez, C.A., Faino, L., Spring In't Veld, D., Smit, S., Zwaan, B.J., and van Kan, J.A. (2016) Comparative genomics of *Beauveria bassiana*: uncovering signatures of virulence against mosquitoes. *BMC Genomics* **17**: 986.

Vanommeslaeghe, K., and MacKerell, A.D. (2012) Automation of the CHARMM general force field (CGenFF) I: bond perception and atom typing. *J Chem Inf Model* **52**: 3144–3154.

Vanommeslaeghe, K., Raman, E.P., and MacKerell, A.D. (2012) Automation of the CHARMM general force field

(CGenFF) II: assignment of bonded parameters and partial atomic charges. *J Chem Inf Model* **52**: 3155–3168.
Vargas, W.A., Sanz-Martin, J.M., Rech, G.E., Armijos-Jaramillo, V.D., Rivera, L.P., Echeverria, M.M., *et al*. (2016) A fungal effector with host nuclear localization and DNA-binding properties is required for maize anthracnose development. *Mol Plant Microbe Interact* **29**: 83–95.
Venard, C., and Vaillancourt, L. (2007) Colonization of fiber cells by *Colletotrichum graminicola* in wounded maize stalks. *Phytopathology* **97**: 438–447.
Voigt, C.A. (2014) Callose-mediated resistance to pathogenic intruders in plant defense-related papillae. *Front Plant Sci* **5**: 168.
Wan, J., Zhang, X.C., and Stacey, G. (2008) Chitin signaling and plant disease resistance. *Plant Signal Behav* **3**: 831–833.
Wang, Z., Zhang, H., Liu, C.Y., Xing, J.J., and Chen, X.L. (2018) A deubiquitinating enzyme Ubp14 is required for development, stress response, nutrient utilization, and pathogenesis of *Magnaporthe oryzae*. *Front Microbiol* **9**: 769.
Weber, R.W.S., Wakley, G.E., Thines, E., and Talbot, N.J. (2001) The vacuole as central element of the lytic system and sink for lipid droplets in maturing appressoria of *Magnaporthe grisea*. *Protoplasma* **216**: 101–112.
Weihmann, F., Eisermann, I., Becher, R., Krijger, J.-J., Hübner, K., Deising, H.B., and Wirsel, S.G.R. (2016) Correspondence between symptom development of *Colletotrichum graminicola* and fungal biomass, quantified by a newly developed qPCR assay, depends on the maize variety. *BMC Microbiol* **16**: 94.
Werner, S., Sugui, J.A., Steinberg, G., and Deising, H.B. (2007) A chitin synthase with a myosin-like motor domain is essential for hyphal growth, appressorium differentiation, and pathogenicity of the maize anthracnose fungus *Colletotrichum graminicola*. *Mol Plant Microbe Interact* **20**: 1555–1567.
Wiederstein, M., and Sippl, M.J. (2007) ProSA-web: interactive web service for the recognition of errors in three-dimensional structures of proteins. *Nucleic Acids Res* **35**: W407–W410.
Yachdav, G., Kloppmann, E., Kajan, L., Hecht, M., Goldberg, T., Hamp, T., *et al*. (2014) PredictProtein-an open resource for online prediction of protein structural and functional features. *Nucleic Acids Res* **42**: W337–W343.
Yu, J.H., Hamari, Z., Han, K.H., Seo, J.A., Reyes-Dominguez, Y., and Scazzocchio, C. (2004) Double-joint PCR: a PCR-based molecular tool for gene manipulations in filamentous fungi. *Fungal Genet Biol* **41**: 973–981.
Zampounis, A., Pigne, S., Dallery, J.F., Wittenberg, A.H., Zhou, S., Schwartz, D.C., *et al*. (2016) Genome sequence and annotation of *Colletotrichum higginsianum*, a causal agent of crucifer anthracnose disease. *Genome Announc* **4**: e00821–e00816.

Supporting Information

Additional Supporting Information may be found in the online version of this article at the publisher's web-site:

Supplemental data file 1. Sheet 1) *C. graminicola* secretome, Sheet 2) orthologues of *M. oryzae* ATMT mutants with virulence defects, Sheet 3) gene clusters encoding secreted proteins, Sheet 4) bioinformatical analyses of Clu5 proteins.

Fig. S1 Analyses of DNA integration in transformants to confirm deletion of *CLU5* and the genes contained within. Each panel provides an overview on the construct used to create the respective mutants. Furthermore, it shows the results of PCR assays for all mutants created and Southern hybridisations of Δ*clu5*, Δ*clu5part*, Δ*clu5a* and Δ*clu5d* mutants validating the respective deletion events.

Fig. S2 Analyses of DNA integration in transformants to confirm reconstitution of the WT allele. Δ*clu5a* and Δ*clu5d* mutants were co-transformed with the respective native gene and pAN7-1. The former, when homologously integrated, replaced the original marker used for the creation of the deletion mutant, whereas the latter should integrate ectopically. (A) PCR assays testing transformants for complementation of Δ*clu5a-2* (GLRG_04686). (B) PCR assays testing transformants for complementation of Δ*clu5d-22* (GLRG_04689). (C) Detached leaf assay testing complementation strains against the corresponding deletion mutants and the WT. Inoculation used 14 d old maize cultivar Mikado and 10^4 conidia per spot. Photos show symptoms at 5 dpi.

Fig. S3 Virulence of deletion mutants of *CLU5* genes on three maize cultivars differing in susceptibility. Representative symptoms are shown that occurred at 4 dpi on detached leaf segments inoculated 14 d after sowing with 10^4 conidia per spot. Susceptibility to the WT decreases from (A) to (C) (Weihmann *et al*., 2016).

Fig. S4 Tests for fitness of deletion mutants of *CLU5* genes. (A) and (B) Mycelial growth *in vitro*. (A) Data points represent the means (n = 5) of radial outgrowth on MM/sucrose (Ø 85 mm) for 8 d. (B) Photographs show representative mycelia at 8 dpi. (C) Formation of conidia formed *in vitro* on OMA plates (Ø 55 mm) in 21 d. Conidia were washed off the plates with 4.5 ml 0.02% Tween 20. Columns represent the means of three plates of which the harvested conidia were counted four times (n = 12). Error bars show SD. None of the mutants differs significantly from WT (unpaired *t*-test, $p < 0.05$).

Fig. S5 Mycelial growth of deletion mutants of *CLU5* genes under stress conditions. PDA plates (Ø 85 mm) amended with 800 μg ml^{-1} Uvitex 2B, 450 μg ml^{-1} Congo Red, 1 M NaCl and 1 M KCl, respectively, were inoculated with mycelial plugs taken from unamended PDA and incubated for the indicated times. In addition, the WT was incubated on unamended PDA.

Fig. S6 Transcript levels of *CLU5* genes. Results of RNAseq analyses for infections on leaves of *Z. mays* cvs. Mo940 and B73, and for conidia formed *in vitro* on OMA and for appressoria differentiated *in vitro* from conidia on polystyrene for 24 hpi. Data of Mo940 were taken from two studies (O'Connell *et al*., 2016; Torres *et al*., 2016). For comparison, transcript levels of the

orthologues in *C. higginsianum* are shown for infection of *A. thaliana* leaves. Data are read counts for infections of Mo940 and *A. thaliana*, FPKM (fragments kb^{-1} of transcript per million mapped reads) for infection of B73 and the *in vitro* differentiated fungus.

Fig. S7 Molecular phylogenetic analyses of Clu5a and Clu5d. The trees are drawn to scale, with branch lengths measured in the number of substitutions per site. Bootstrap tests (1000x) analysed the percentage of trees in which the associated taxa clustered together, which is shown at the branches. (A) Clu5a. MEGA6 computed the tree based on the Le Gascuel 2008 model. The tree with the highest log likelihood (−1303.5493) is shown unrooted. A discrete Gamma distribution was used to model evolutionary rate differences among sites (5 categories (+G, parameter = 1.0002)). The analysis involved 23 amino acid sequences. There were 53 positions in the final dataset. (B) Clu5d. MEGA6 computed the tree based on the Whelan and Goldman + Freq. model. The tree with the highest log likelihood (−4217.8559) is shown unrooted. A discrete Gamma distribution was used to model evolutionary rate differences among sites (5 categories (+G, parameter = 1.6875)). The rate variation model allowed some sites to be evolutionarily invariable ([+I], 16.3802% sites). The analysis involved 21 amino acid sequences. There were 204 positions in the final dataset.

Fig. S8 Staining of infection structures formed *in vitro* by Δ*clu5a* mutants. Infection structures of mutants and the WT developed on glass slides in moistened petri dishes at R.T. in the dark for 48 hpi before treatment with staining solutions. For the visualization of lipid droplets specimens were stained with 500 μg ml^{-1} Nile red (Acros Organics, Geel, Belgium) in acetone for 15 min and washed with PBS for 10 min. For the visualization of cell walls, specimens were stained for 1 min with Calcofluor white stain containing 0.5 g l^{-1} Calcofluor white M2R and 0.25 g l^{-1} Evans blue in 5% potassium hydroxide (Sigma-Aldrich, München, Germany) and shortly washed with H_2O_{bidest}.

Fig. S9 Formation of hydrogen peroxide on maize leaves infected with Δ*clu5a* and Δ*clu5d* mutants. Cultivar Mikado was inoculated with 10^4 conidia per site, 14 d after sowing. LM of tissue samples harvested at 2 dpi and stained with DAB. Insertions show typical appressoria. Bars represent 50 μm.

Fig. S10 Pathogenesis on maize leaves of Δ*clu5* and Δ*clu5part* mutants. Cultivar Mikado was inoculated with 10^4 conidia per site, 14 d after sowing. Micrographs obtained by LM after staining with Aniline blue show fungal development in the epidermal layer at the indicated times. P = biotrophic primary hypha, S = necrotrophic secondary hypha, black arrowheads mark appressoria.

Fig. S11 Cytorrhysis and cavitation of appressoria formed *in vitro* by Δ*clu5a* and Δ*clu5d* mutants. Infection structures developed on plastic sheets for 48 h before treatment with 1.2 M PEG 200, 18 M ethane-1,2-diol, and 5 M NaCl respectively. Micrographs were obtained by LM.

Fig. S12 Scanning electron microscopy of appressoria formed *in vitro* by Δ*clu5a* and Δ*clu5d* mutants. Surface topography of melanised appressoria developed on cover slips by each, the WT, Δ*clu5a-2*, Δ*clu5a-4*, Δ*clu5d-17* and Δ*clu5d-22* mutants respectively.

Fig. S13 Atomic force microscopy of appressoria formed *in vitro* by Δ*clu5a* mutants. Surface topography and local elasticity distribution of three melanised appressoria developed on cover slips by each, the WT, Δ*clu5a-2* and Δ*clu5a-4* mutants respectively.

Table S1 Oligonucleotides used.